Deletion and single nucleotide substitution at G:C in the kidney of *gpt* delta transgenic mice after ferric nitrilotriacetate treatment

Li Jiang,[1] Yi Zhong,[1] Shinya Akatsuka,[1] Yu-Ting Liu,[1] Khokon Kumar Dutta,[1] Wen-Hua Lee,[1] Janice Onuki,[1,2] Ken-ichi Masumura,[3] Takehiko Nohmi[3] and Shinya Toyokuni[1,4]

[1]Department of Pathology and Biology of Diseases, Graduate School of Medicine, Kyoto University, Kyoto 606-8501; [2]Laboratory of Biochemistry and Biophysics, Butantan Institute, São Paulo, SP, Brazil; [3]Division of Genetics and Mutagenesis, National Institute of Health Sciences, Tokyo 158-8501, Japan

(Received June 7, 2006/Revised July 13, 2006/Accepted July 14, 2006/Online publication August 23, 2006)

An iron chelate, ferric nitrilotriacetate (Fe-NTA), induces oxidative renal proximal tubular damage that subsequently leads to a high incidence of renal cell carcinoma in rodents, presenting an intriguing model of free radical-induced carcinogenesis. In the present study, we used *gpt* delta transgenic mice, which allow efficient detection of point mutations and deletions *in vivo*, to evaluate the mutation spectra, in association with the formation of 8-oxoguanine and acrolein-modified adenine during the first 3 weeks of carcinogenesis. Immunohistochemical analysis revealed the highest levels of 8-oxoguanine and acrolein-modifed adenine in the renal proximal tubules after 1 week of repeated administration. DNA immunoprecipitation and quantitative polymerase chain reaction analysis showed that the relative abundance of 8-oxoguanine and acrolein-modified adenine at the *gpt* reporter gene were increased at the first week in the kidney. Similarly, in both 6-thioguanine and Spi$^-$ selections performed on the renal specimens after Fe-NTA administration, the mutant frequencies were increased in the Fe-NTA-treated mice at the first week. Further analyzes of 79 mutant clones and 93 positive plaques showed a high frequency of G:C pairs as preferred targets for point mutation, notably G:C to C:G transversion-type mutation followed by deletion, and of large-size (>1 kilobase) deletions with short homologous sequences in proximity to repeated sequences at the junctions. The results demonstrate that the iron-based Fenton reaction is mutagenic *in vivo* in the renal tubular cells and induces characteristic mutations. (*Cancer Sci* 2006; 97: 1159–1167)

Oxidative stress is associated with a variety of pathological phenomena, including infection, inflammation, ultraviolet- and γ-irradiation, overload of transition metals and certain chemical agents.[1] Many epidemiological studies have demonstrated a close association between chronically oxidative conditions and carcinogenesis. For example, chronic tuberculous pleuritis causes a high incidence of malignant lymphoma;[2] asbestosis (asbestos fibers are rich in iron),[3] is often associated with mesothelioma and lung carcinoma;[4] chronic *Helicobacter pylori* infection is associated with a high incidence of gastric cancer;[5,6] the incidence of colorectal cancer is increased in ulcerative colitis;[7,8] a high risk for heptocellular carcinoma is observed in patients with genetic hemochromatosis, an iron overload disease;[9,10] severe burns by ultraviolet radiation is a risk factor for skin cancer;[11,12] and γ-irradiation causes a high incidence of leukemia.[13] At least under these circumstances, and probably in other types of carcinogenesis as well, oxidative stress appears to play a major role in human carcinogenesis.

An iron chelate, ferric nitrilotriacetate (Fe-NTA), causes oxidative renal proximal tubular injury via the Fenton reaction, and this injury ultimately leads to a high incidence of renal cell carcinoma in mice[14] and rats[15] after repeated intraperitoneal administration. This is an intriguing model in the following respects: (1) more than half of the induced tumors metastasize to the lung and/or invade the peritoneal cavity, resulting in animal mortality;[16] (2) convincing evidence exists regarding the involvement of free radical reactions in the carcinogenic process, including not only an increase in covalently modified macromolecules (oxidatively modified DNA bases[17] and lipid peroxidation products)[18,19] but also preventive effects of α-tocopherol fortification against carcinogenesis;[20] (3) genetic changes in the *p16^{INK4a}* tumor suppressor gene, especially homozygous deletions[21,22] and expressional alteration of several key genes, including annexin 2[23] and thioredoxin binding protein-2,[24] have been observed.

Fe-NTA itself is Ames test-negative,[14] but is positive in other cell culture systems detecting mutations.[25,26] Thus far, its mutation spectrum has not been comprehensively studied. Since the Ames test is a system involving prokaryotes, an assay system with the ability to detect mutations under *in vivo* conditions in which eukaryotic DNA repair mechanisms, metabolic pathways and other physiological systems are operative would offer significant advantages with respect to reliability. Based on this premise, several transgenic mouse mutagenesis assay systems have been developed, including Muta mice,[27] Big Blue mice[28] and HITEC mice.[29] These systems employ a recoverable transgenic lambda phage vector containing a reporter gene from bacteria. However, these systems all have the limitation that large deletions cannot be efficiently detected. We have developed a novel mutagenesis test system named *gpt* delta transgenic mice, which are transgenic for the *lambda EG 10* gene containing the *gpt* gene of *Escherichia coli*.[30] An important feature of this system is that both point mutations and large deletions can be tested concurrently in the targeted organs of the mice; point mutations are detected by 6-thioguanine (6-TG) selection and deletions larger than 1 kb can be identified by Spi$^-$ (sensitive to P2 interference) selection. Thus far, various mutagens, including γ-ray irradiation, UVB, mitomycin C and PhIP, have been studied by using this *in vivo* system.[31]

In the present study, we used *gpt* transgenic mice to investigate the early genetic changes in Fe-NTA-induced renal carcinogenesis. Furthermore, we studied the relative abundance of two different types of DNA base modifications in several limited genomic loci with a novel technique called DNA immunoprecipitation (DnaIP), which selectively collects enzyme-digested DNA fragments

[4]To whom correspondence should be addressed.
E-mail: toyokuni@path1.med.kyoto-u.ac.jp
Abbreviations: acrolein-dA, acrolein-modified 2′-deoxyadenosine; APNH, aminophenylnorharman; bp, base pairs; Cm, chloramphenicol; dCTP, 2′-deoxycytidine triphosphate; DnaIP, DNA immunoprecipitation; EDTA, ethylenediaminetetraacetic acid; FaPy, formamidopyrimidine; Fe-NTA, ferric nitrilotriacetate; MF, mutant frequency; MMC, mitomycin C; 8-OHdG, 8-hydroxy-2′-deoxyguanosine; PCR, polymerase chain reaction; PhIP, 2-amino-1-methyl-6-phenylimidazo[4,5-b]pyridine; 6-TG, 6-thioguanine; UVB, ultraviolet B; TE, Tris-EDTA.

doi: 10.1111/j.1349-7006.2006.00301.x

containing the target oxidative DNA base modification with specific monoclonal antibody. The present study for the first time revealed characteristics of the mutation spectrum in the kidney following repeated episodes of the Fenton reaction.

Materials and Methods

Animals and chemicals. *Gpt* delta C57BL/6 J transgenic mice were provided by Dr Takehiko Nohmi (Division of Genetics and Mutagenesis, National Institute of Health Sciences, Tokyo, Japan) and maintained in Kyoto University under specific-pathogen free and light-, temperature- and humidity-controlled conditions. The animal experiment committee of the Graduate School of Medicine, Kyoto University, approved the present experiments. $Fe(NO_3)_39H_2O$ was obtained from Wako (Osaka, Japan). Nitrilotriacetic acid, disodium salt, was purchased from Nacalai Tesque (Kyoto, Japan). Fe-NTA was prepared immediately before use as described previously.[18] A total of 12 4-week-old male mice were used; nine mice were subjected to repetitive Fe-NTA administration and three mice were used as untreated controls. Mice were injected intraperitoneally with 3 mg iron/kg of Fe-NTA daily for three days, and the dose was increased to 5 mg iron/kg of Fe-NTA from the fourth day according to the established carcinogenesis protocol.[16] The injections were performed five times a week at approximately 10.00 hours. The animals were killed 48 h after the final administration. Both kidneys and the central lobe of the liver were immediately excised. Half of one kidney and a portion of the liver were used for histological and immunohistochemical analysis, and the rest of the kidney was frozen in liquid nitrogen and stored at −80°C for mutational analyzes.

Monoclonal antibodies. Monoclonal antibody N45.1 recognizing 8-hydroxy-2′-deoxyguanosine (8-OHdG)[32] and monoclonal antibody mAb21 recognizing acrolein-2′-deoxyadenosine adduct (acrolein-dA)[33] were used.

Histological and immunohistochemical analyzes. Kidney specimens were fixed with phosphate-buffered 10% formalin and embedded in paraffin, cut at 3-μm thickness and stained with hematoxylin and eosin staining. For immunohistochemical analyzes, the avidin-biotin complex method with peroxidase was used as described previously.[32,33]

DNA immunoprecipitation and quantitative PCR analysis. To evaluate the relative abundance of Fe-NTA-induced oxidative DNA base modifications (8-OHdG and acrolein-dA) at desired genomic loci, we developed a technique designated as DnaIP (DNA immunoprecipitation).[34] More details will be published elsewhere.[35] Briefly, genomic DNA was extracted from each kidney of *gpt* delta transgenic mice with the NaI method (Wako) using argon gas-saturated buffer to avoid further oxidation during the extraction procedures.[36] Twenty μg of genomic DNA was digested with *Hae*III (TakaraBio, Shiga, Japan), and incubated with each antibody (10 μg of N45.1 or 2 μg of mAb21) in 10 mM phosphate-buffered saline, pH 7.4, containing 0.1% bovine serum albumin, for 3 h at 4°C in a 900-μL volume. The mixture was then incubated with 100 μL of Dynabeads M-280 sheep antimouse IgG (Dynal, Oslo, Norway) for another 3 h, washed sequentially with four different buffers (buffer 1: 0.1% sodium deoxycholate, 1% Triton X-100, 1 mM EDTA, 50 mM HEPES-KOH, 140 mM NaCl, pH 7.5; buffer 2: 0.1% sodium deoxycholate, 1% Triton X-100, 1 mM EDTA, 50 mM HEPES-KOH, 500 mM NaCl, pH 7.5; buffer 3: 0.1% sodium deoxycholate, 0.5% Nonidet P-40, 1 mM EDTA, 250 mM LiCl, 10 mM Tris-HCl, pH 8.0; and buffer 4: 1 × TE). Beads-bound DNA was recovered by incubating the beads with 80 μL of elution buffer (10 mM EDTA, 1% SDS, 50 mM Tris-HCl, pH 8.0) at 65°C for 10 min, and was amplified twice by PCR after ligation to an adaptor (sense, 5′-OH-GGAATTCGGCGGCCGCGGATCC-3′; antisense, 5′-GGATCC-GCGGCCGCCG-3′; sense oligonucleotides were used as primers for amplification), treated with exonuclease I (TakaraBio) and purified with phenol-chloroform extraction. The purified products were subjected to Real-Time PCR (7300 Real Time PCR System, Applied Biosystems, Tokyo) using Platinum SYBR Green qPCR SuperMix UDG (Invitrogen, Tokyo). The primer pairs used were as follows: *gpt*, forward-5′-GCCTTCTGAACAATGGAAAGG-3′, reverse-5′-CGTGATCGTAGCTGGAAATAC-3′ (125 bp); β-*actin*, forward-5′-TCCAACAAACCAAGAGAAATCC-3′, reverse-5′-CGACCTCTGAAACAATTCTGGT-3′ (108 bp); C15-49–5 (chromosome 15, extrageneic region), forward-5′-TGGTACCTGAGT-AAGGCAAGGT-3′, reverse-5′-CCCACTTGTGATTGCTTTCTTC-3′ (107 bp); C16-47–2 (chromosome 16, extrageneic region): forward-5′-CACACACACATGCACACTGTACT-3′, reverse-5′-GCATTTCTCCTCACATTCAGACT-3′ (114 bp); C16-47–5 (chromosome 16, extrageneic region): forward-5′-CCAATTGG-AGCTAACAGAAACC-3′, reverse-5-AGCTGGTCAACTGCC-TACTCTC-3′ (125 bp). These three extrageneic areas were selected based on our observations that chromosome 15 is peripherally located and chromosome 16 is centrally located in the murine renal tubular cells at interphase.[35]

***In vitro* phage packaging.** Genomic DNAs were extracted with the phenol-chloroform extraction protocol.[37] Trangenic *lambda EG10* DNA was rescued from the host genomic DNA using Transpack Packaging Extract (Stratagene, La Jolla, CA) according to the manufacturer's instructions.[30]

Mutation analysis. The 6-TG mutation assay protocol has been described elsewhere.[38–40] Briefly, rescued phage was infected into YG 6020 *E. coli* expressing Cre enzyme, converted into a plasmid carrying the *Cm-resistance* gene and *gpt* gene, and poured on plates containing chloramphenicol (Cm) with or without 6-TG. The positive clones carrying the mutant *gpt* gene were obtained from 6-TG selection plates by incubating at 37°C for 96 h. Selected clones were confirmed again by plating on 6-TG selection plates. The whole *gpt* sequence was amplified from positive clones and identified by sequencing with an ABI PRIZM 377 sequencer. The primers used for amplifying and sequencing were as follows: forward-5′-GCGCAACCTATTTTCCCCTCGA-3′ and reverse-5′-TGGAAACTATTGTAACCCGCCTG-3′. The same primer pair was used for direct sequencing.[41] *E. coli* XL1-Blue MRA and XL1-Blue MRA (P2) were infected with the packaged phage. *E. coli* XL1-Blue MRA was poured onto NZY plates and XL1-Blue MRA (P2) was poured onto I-trypticase agar plates. Plaques that grew on the XL1-Blue MRA (P2) plates were selected and further confirmed with *E. coli* XL1-Blue MRA, *E. coli* WL95 (P2) and XL1-Blue MRA (P2). Positive plaques were recovered and used for determining the deletion position of the *red/gam* gene. Clones or plaques were counted for determining mutant frequencies (MFs). MFs were calculated by using established methods as described previously.[30,42,43]

Hybridization assay and PCR analysis for Spi⁻ mutant analysis. A protocol for Southern blot analysis for Spi⁻ (sensitive to P2 interference) mutants has been established.[43] Seventeen oligomers located within ~14 kb flanking sequence of the *red/gam* gene were used as probes for identifying the deletion junctions. These oligomers were named 18874R, 19258R, 20341R, 21328R, 22556R, 22869R, 23921R, 24858R, 25389F, 26704F, 27096F, 28165F, 29290F, 30104F, 31070F, 31879F and 32890F according to their position as described.[43] The oligomers were spotted onto Hybond™-N⁺ membrane (Amersham) and cross-linked with UV. PCR products, which were amplified by primer 18874R and 32890F using positive individual plaques as templates, were labeled with (α-^{32}P) dCTP using the Megaprime DNA labeling System (Amersham). The membranes were incubated with labeled PCR products at 50°C overnight, washed three times and exposed to BioMax film (Kodak, New York, NY). Deleted regions were located within those oligomers whose signals could not be observed on the film. The nearest primers were selected for PCR amplification and the PCR products were subjected to sequencing to determine the exact deletion junction.

doi: 10.1111/j.1349-7006.2006.00301.x

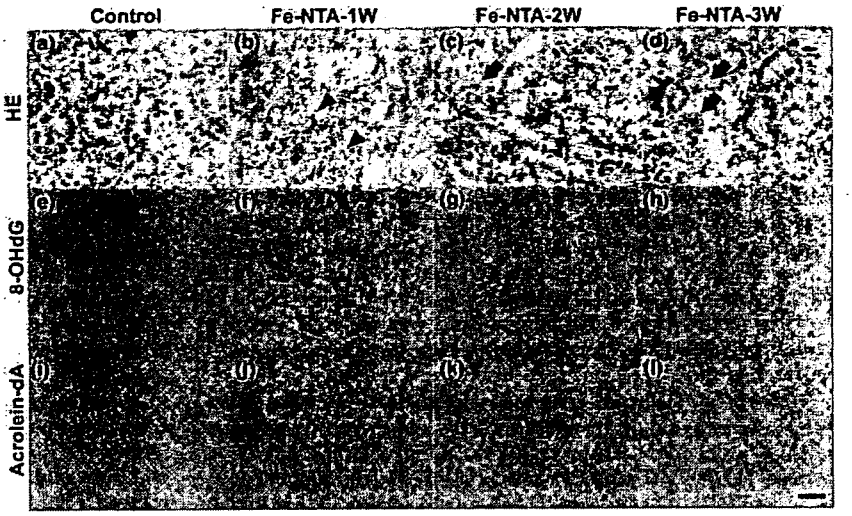

Fig. 1. Immunohistochemical analysis of 8-hydroxy-2'-deoxyguanosine (8-OHdG) and acrolein-modified 2'-deoxyadenosine after repeated administration of ferric nitrilotriacetate (Fe-NTA). (a–d) Hematoxylin and eosin (HE) staining. Regenerative proximal tubular cells were prominent at the first week, together with some necrotic cells (b, ▶). At the second and third week, necrotic cells were no longer observed but increasing numbers of karyomegalic cells (c and d, ▶) appeared. (e–h) Immunohistochemistry of 8-OHdG. Nuclear immunopositivity was observed after Fe-NTA administration, with the highest level after repeated administration for 1 week (f). (i–l) Immunohistochemistry of acrolein-dA. Nuclear immunopositivity was observed after Fe-NTA administration with that of repeated administration of 1 week the highest level (j). Refer to the Materials and Methods section for details (bar in l, 50 μm).

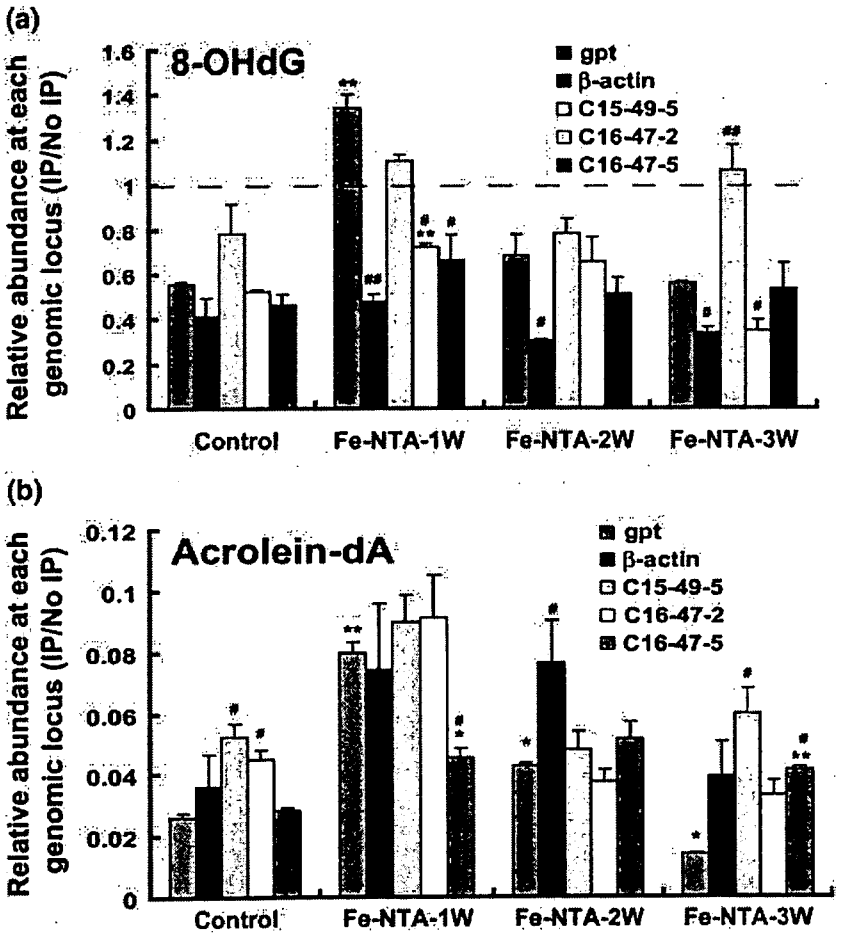

Fig. 2. Real-time polymerase chain reaction (RT-PCR) analysis after DNA immunoprecipitation for quantitation of oxidatively modified DNA bases at specific genomic loci. Renal genomic DNA was digested with *Hae*III and subjected to immunoprecipitation (IP) with specific monoclonal antibodies against 8-hydroxy-2'-deoxyguanosine (8-OHdG) and acrolein-dA. The recovered DNA fragments were amplified after ligation to an adapter and were used as substrates for RT-PCR analyses of *gpt*, *β-actin* and three extrageneic regions at chromosome 15 or 16. Data are shown as relative abundance of PCR products amplified from recovered genomic DNA by IP per those amplified from the original genomic DNA in the same amounts. (a) 8-OHdG. (b) Acrolein-dA. Refer to the Materials and Methods section for details ($N = 3$, means ± SEM; $^{*}P < 0.05$, $^{**}P < 0.01$ versus untreated control kidney at the same genomic region; $\#P < 0.05$, $\#\#P < 0.01$ versus *gpt* locus data of the same treatment group).

Statistical analysis. Statistical analyzes were performed with an unpaired *t*-test, which was modified for unequal variances when necessary.

Results

Renal histology after repeated Fe-NTA administration. As shown in Fig. 1a, no significant histological changes were observed in the kidney of the untreated control group. In contrast, pyknotic nuclei of proximal tubular cells revealing degeneration were scattered in the kidney of mice after 1 week of Fe-NTA treatment (Fig. 1b). Degenerative tubular cells were no longer observed there after 2 or 3 weeks of repeated Fe-NTA treatment, but atypical regenerative cells with a large nucleus containing prominent nucleoli were gradually increased (Fig. 1c,d). In either case, histological evaluation of the liver showed no apparent alterations (data not shown).

Oxidative DNA damage induced by repeated Fe-NTA administration. Two major oxidative DNA base modifications, 8-OHdG and acrolein-dA, were evaluated with immunohistochemistry and DnaIP. Intense diffuse nuclear immunostaining of 8-OHdG and acrolein-dA was prominent in the renal proximal tubules after repeated Fe-NTA administration for 1 week, and gradually decreased thereafter (Fig. 1e–l). To assess whether these oxidative modifications were increased in the *gpt* gene locus, quantitative PCR analysis after DnaIP was performed. The *gpt* reporter gene locus after 1 week of repeated Fe-NTA administration showed higher amounts of 8-OHdG and acrolein-dA than that in the untreated control group. Similar patterns were also observed in the other loci examined, but the *gpt* locus was the most sensitive at the first week (Fig. 2), consistently with the immunohistochemical data (Fig. 1e–l).

Fe-NTA-induced mutant frequencies in *gpt* and *red/gam* genes. We then investigated the reporter genes, *gpt* and *red/gam*, to analyze Fe-NTA-induced mutations using the 6-TG and Spi$^-$ selection systems. In both 6-TG and Spi$^-$ selections, the mutation frequencies were significantly increased (2.44-fold increase in 6-TG selection and 1.72-fold increase in Spi$^-$ selection) after 1 week of repeated Fe-NTA administration (Fig. 3), which was consistent with the results of immunohistochemistry (Fig. 1e–l) and DnaIP (Fig. 2).

Fe-NTA-induced *gpt* gene mutations. To further characterize the exact *gpt* mutations caused by Fe-NTA, 79 mutant clones, in which 69 clones were from Fe-NTA-treated mice and 10 from untreated control mice, were analyzed (Table 1 and Fig. 4). Among the mutations induced by Fe-NTA, 75.4% (52/69) were single base substitutions, of which more than half (32/52 = 61.5%) occurred at G:C base pairs, whereas GC content of *gpt* gene was 46.6%. Among the Fe-NTA-induced substitutions, 40.4% (21/52) were transitions, including G:C to A:T (13/21) and A:T to G:C (8/21), whereas the rest of substitutions (31/52 = 59.6%) were transversions, including G:C to T:A (5/31), G:C to C:G (14/31), A:T to T:A (4/31) and A:T to C:G (8/31) (Table 1). In addition, 17.4% (12/69) of mutant clones were identified as carrying single- or mutiple-base deletions. Among them, 9/12 were single-base deletions, which occurred preferentially at repeated sequences (Table 1 and Fig. 4). Four insertional mutations and one tandem base substitution were also observed. In contrast, analyses of a total of 10 clones from the untreated control kidney showed that 8/10 were single-base substitutions with a single-base deletion and an insertion. In either case, complex mutations were not observed. Therefore, the results indicated that Fe-NTA-induced *gpt* gene mutation preferentially consisted of single-base substitutions occurring at G:C base pairs, in which transversions were more frequent than transitions (Table 1).

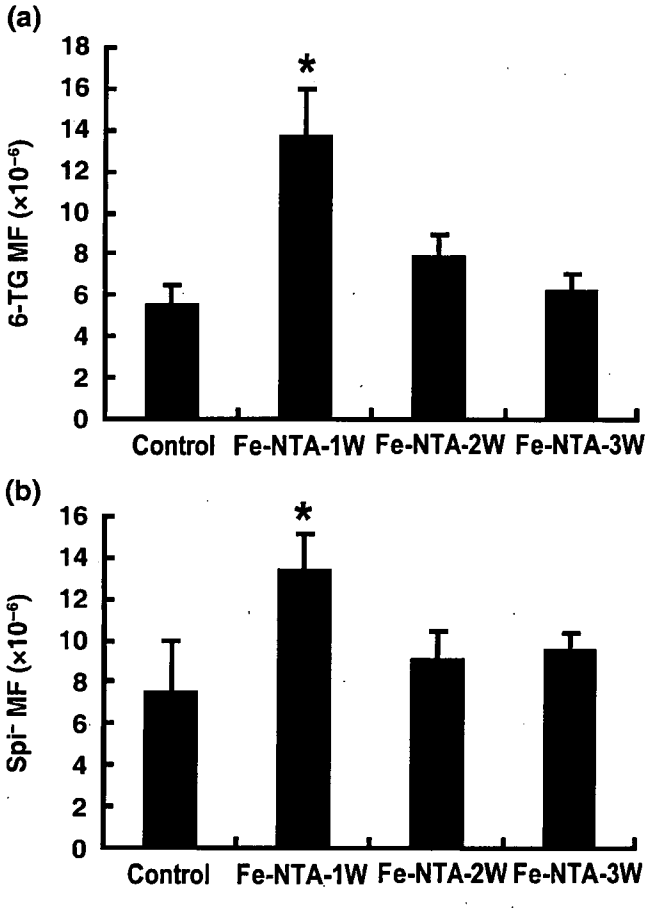

Fig. 3. Mutant frequency (MF) of 6-TG and Spi$^-$ seletion. 6-TG selection was used for the detection of base substitutions in the *gpt* gene; Spi$^-$ selection was used for the detection of large-size deletions. Refer to the Materials and Methods section for details. ($N = 3$, means ± SEM; $^*P < 0.05$, $^{**}P < 0.01$ *versus* untreated control kidney).

Fe-NTA-induced Spi$^-$ mutations. To characterize the Spi$^-$ mutations induced by Fe-NTA, 93 positive plaques obtained from either the kidneys of Fe-NTA-treated mice or untreated control mice were screened by Southern blot analysis followed by sequencing that resulted in the confirmation of 21 large-size deletions (Fig. 5a). Large-size deletions were at first roughly positioned on ~14 kb of sequence spanning the *red/gam* gene by the use of 17 different oligomers as probes. We detected signals for all the 17 oligomer probes in the blot with hybridization to the wild-type *lambda EG 10* (Fig. 5b i). Signals for certain oligomers were absent with Spi$^-$ mutant plaques containing large-size deletions, as shown in Fig. 5(b ii–iv). Most of the large deletions induced by Fe-NTA were more than 1 kb in size (Class I mutation,[31] (Fig. 5a). Furthermore, the majority of them (70.6%) had short homologous sequences of 1–6 bp at the junctions (Class I-A), and in many cases showed three bp or longer running sequences at the junction or its vicinity. Five cases of large-size deletions were accompanied by simultaneous single-base deletion in the *red/gam* gene (Fig. 5a).

Discussion

In the present experiments we have for the first time studied the mutation spectrum of the Fenton reaction-based renal tubular damage in a model of oxidative stress-induced carcinogenesis mediated by Fe-NTA. We intentionally avoided the acute periods for evaluation because of the abundance of necrosis and apoptosis,[20,44] and thus used the subacute phase when the majority of the tubular cells become resistant to oxidative stress with rare cell death present (Fig. 1b–d), though mutation spectrum might be slightly different between the acute and subacute phases. The accumulation of two different kinds of oxidative DNA base modifications, 8-OHdG and acrolein-dA, was most evident with immunohistochemistry after the first week of repeated administration of Fe-NTA and gradually decreased thereafter (Fig. 1e–l). This is probably due to the activation in the cellular metabolic pathways for those either suppressing the Fenton reaction or promoting DNA repair mechanisms. It is also possible that cellular selective processes worked to remove heavily damaged cells.

Gpt delta transgenic mice are an established model for analyzing mutations *in vivo*, and have been used to analyze several possible mutagens.[31] Here we have used a technique designated as DnaIP to evaluate the relative abundance of the two DNA base modifications at the *gpt* loci. Approximately 80 copies of the

doi: 10.1111/j.1349-7006.2006.00301.x

Table 1. Spectrum of Fe-NTA-induced mutations in the kidney of *gpt* delta transgenic mice

Mutation type	Nucleotide position	Sequence change	Amino acid change	Fe-NTA			Control
				1w	2w	3w	
Transition					30.4%		50.0%
G:C–A:T	27	G–A	Trp–STOP	1			
	39	G–A	Gln–Gln				1
	64	C–T	Arg–STOP	1			1
	110	G–A	Arg–His	5			1
	113	G–A	Arg–His				1
	116	G–A	Arg–Arg			1	
	128	G–A	Val–Met		1	1	
	287	C–T	Thr–Ile	1			
	356	G–A	Arg–His		1		
	447	C–T	Ile–Ile			1	
A:T–G:C	2	T–C	Met–Thr		1		
	25	T–C	Trp–Ser	1	2		
	188	A–G	Tyr–Cys		1		
	275	A–G	Asp–Gly				1
	307	A–G	Met–Val	1			
	410	A–G	Gln–Arg		1		
	415	T–C	Trp–Arg			1	
Transversion					44.9%		30.0%
G:C–T:A	3	G–T	Ser–Ile		1		
	110	G–T	Arg–His		1		
	115	G–T	Gly–Cys	1			
	189	C–A	Tyr–STOP	1			
	324	C–A	His–Gln				1
	418	G–T	Asp–Try	1			
G:C–C:G	109	C–G	Arg–Gly			1	
	125	C–G	Pro–Arg			1	
	238	G–C	Asp–His			1	
	297	G–C	Ala–Ala	2			
	413	C–G	Pro–Arg	2	1		
	414	G–C	Pro–Pro	2			
	427	G–C	Val–Leu	1		1	
	430	G–C	Val–Leu	2			1
A:T–T:A	52	A–T	Lys–STOP	1			
	66	A–T	Arg–Arg			1	
	179	T–A	Ile–Asn		1	1	
A:T–C:G	94	A–C	Ile–Leu		1		
	133	T–G	Phe–Val		1		
	134	T–G	Gly–STOP		1	1	
	146	A–C	Glu–Ala		1		
	286	A–C	Thr–Pro	1		1	
	315	A–C	Pro–Pro	1			
	375	T–G	Tyr–STOP				1
Deletions					17.4%		10.0%
1 base pair	8–12	AAAAA–AAAA		1	3	1	1
	88–90	AAAGG–AAGG				1	
	423–425	GGGCG–GGCG		1			
	430	TCGTA–TCTA				1	
	437	CGTCC–CGCC				1	
>2 base pairs	156–162	ATTCGTCATGT–ATCG			1		
	170–171	TACCG–TAG			1		
	252–253	TTCATC–TTTC			1		
Insertions					5.7%		10.0%
	74–75	CCTT–CCAATT				1	
	122–123	GTAC–GTTAC		1			
	310–311	ATCC–ATTCC			1	1	
	440–441	CCGC–CCCGC					1
Other					1.4%		0.0%
CC–AG	124–125	TACCGG–TAAGGG			1		

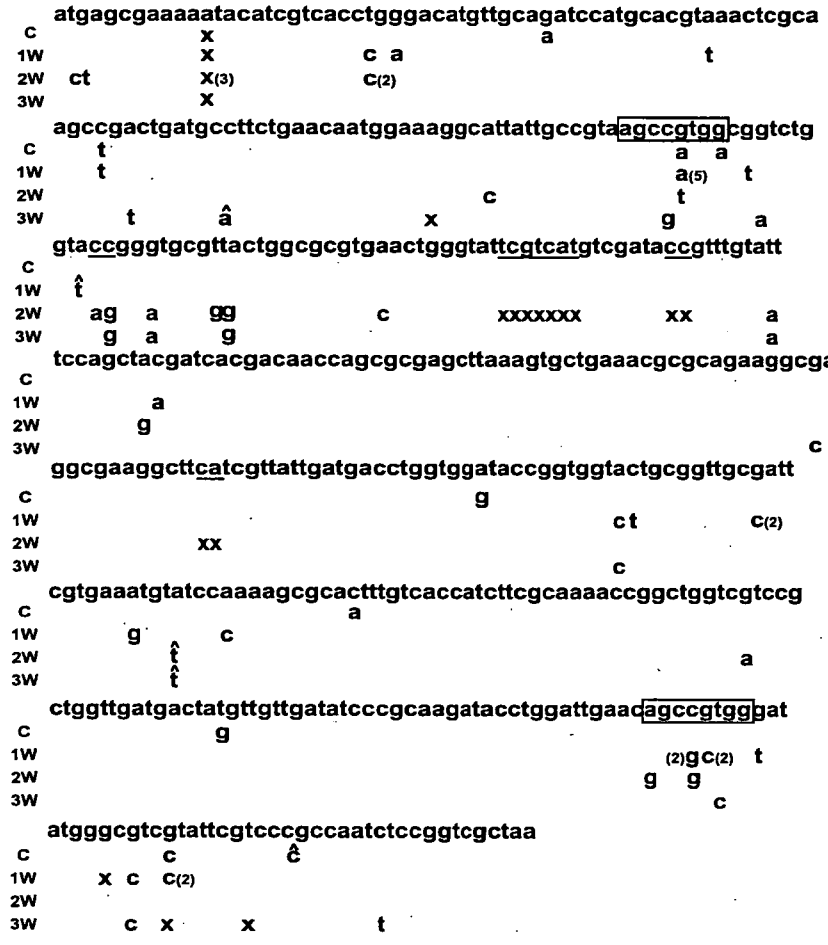

Fig. 4. The position of point mutations in the *gpt* gene. Refer to the Materials and Methods section for details (x, deletion; ^, insertion; underline, more than one base pair deletion within the same case; the number in parenthesis indicates the multiplicity of the same mutation. Square (in one letter), mutation-prone area with the same sequence.

transgenes are included per haploid genome in the *gpt* delta transgenic mice.[30] Among genomic loci examined, including β-actin and three extrageneic regions, the *gpt* loci showed the highest level of 8-OHdG and acrolein-dA after one week of repeated Fe-NTA administration (Fig. 2). This consistency with the immunohistochemical data demonstrates that the transgenic *gpt* loci are indeed vulnerable and suitable for mutational analyzes. We believe that the high copy number of the *gpt* gene contained in these mice is at least partially responsible for this reliable sensitivity. In contrast to the findings at one week, certain extrageneic loci showed significantly higher levels of DNA base modifications than the *gpt* gene locus at other time points, suggesting that further studies would be necessary to elucidate the principles governing the distribution of oxidative DNA base modifications over the whole genome.[35,45]

Mutation frequencies both for the 6-TG selection and Spi$^-$ selection also were the highest at the first week of repeated Fe-NTA administration (Fig. 3). This confirms the usefulness of 8-OHdG and acrolein-dA, which were detected both by immunohistochemistry and DnaIP, as reliable markers of mutation. In 22.7% of the Spi$^-$ plaques after Fe-NTA treatment, large-size deletions (>1 kb) were observed and most of them were class I-A mutants (Fig. 5). This preference for large-size deletions with short homologous sequences at the junctions might be a prominent feature of the results obtained in this renal carcinogenesis model in that the patterns of Spi$^-$ mutations are similar to that of the untreated colon.[31] With γ-rays, shorter deletions than 1 kb are prominent; with UVB and MMC, large-size deletions with or without short homologous sequences at the junctions are more frequently observed (>40%); whereas with PhIP and APNH, large-size deletions were rare.[31]

In the Fe-NTA-induced renal cell carcinoma of rats, homozygous deletion of the *p16^{INK4A}* tumor suppressor gene was frequently observed,[21] and the allelic loss of this locus was observed at a high frequency one to three weeks after the repeated administration of Fe-NTA in rats.[22] We believe that the iron-mediated Fenton reaction is mainly responsible for this characteristic deletion. Short deletions were also increased after Fe-NTA administration (Table 1). Probably, the free radical reaction associated with iron is distinct from the reactions associated with other agents studied so far in the *gpt* lambda transgenic mice in that this is a universal reaction, though exaggerated through iron overload, involving the generation of hydroxyl radical and lipid peroxidation products. This kind of reaction is always taking place in the body under conditions of normal metabolism associated with oxygen consumption and, though it results in only minor consequences under physiological conditions, can be a driving force of carcinogenesis.

The mutation spectrum detected in the *gpt* gene was also quite distinctive. G:C pairs were the preferred bases for mutation, and especially G:C to C:G transversion-type mutation was characteristic (Fig. 4 and Table 1). This type of mutation was observed in PhIP and MMC as a minor type, but has not been reported as a major type of mutation (Table 2). We observed a low incidence of G:C to T:A transversion-type mutation that results from

doi: 10.1111/j.1349-7006.2006.00301.x

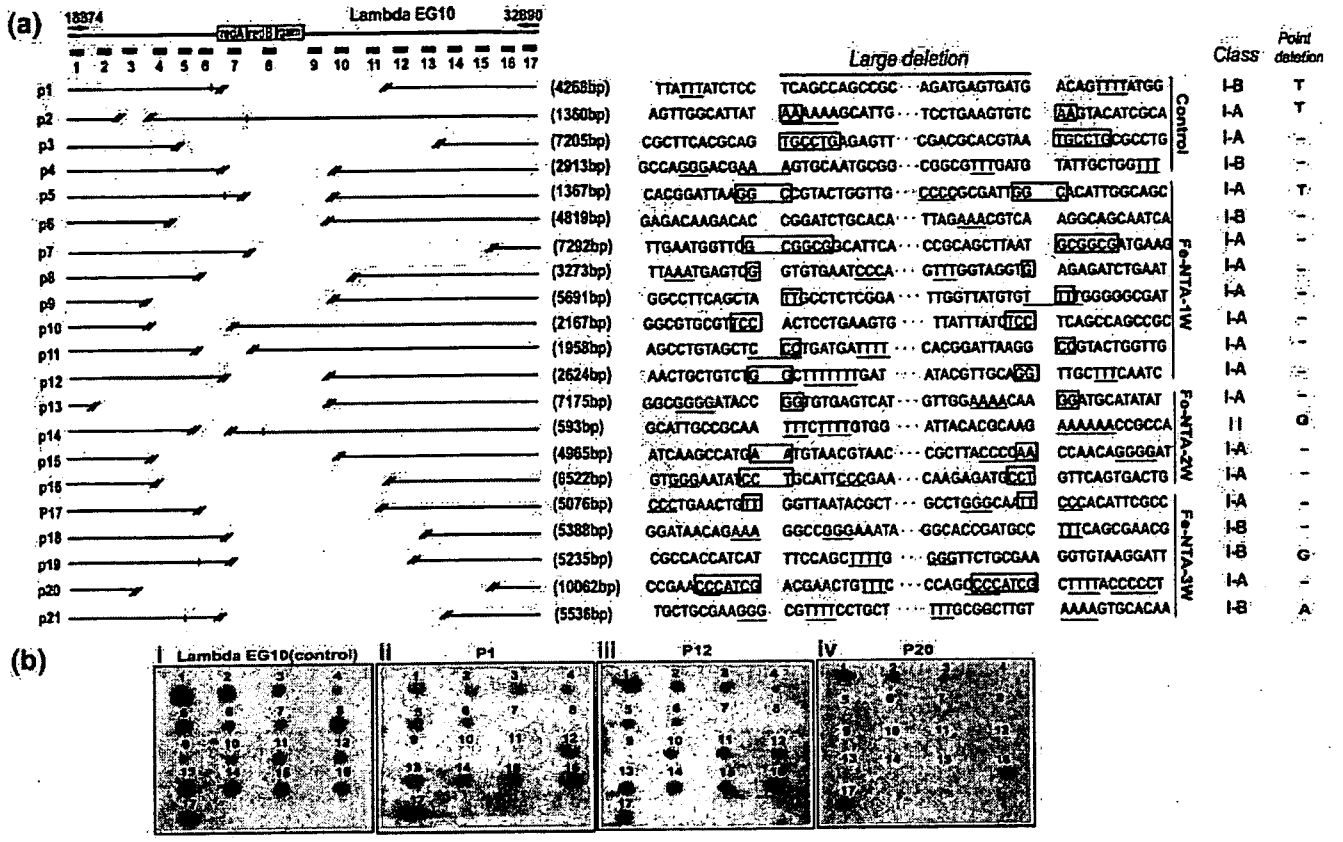

Fig. 5. Size and position of large-size deletions after Spi⁻ selection with each junctional sequence. (a) Summary of the strategy and the observed deletions. P1–P4, untreated control; P5–P21, ferric nitrilotriacetate (Fe-NTA)-induced deletions. Blank areas between two double-dash lines indicate large-size deletions; short longitudinal lines indicate accompanying 1-base deletion; □, short homologous sequence; underline, short run more than 3 bp. Classification of the deletion type was done as described.[31] (b) Representative results of Southern blotting analysis for screening the deleted positions. Arabic numerals (1–17) indicate the probes used as described in the Materials and Methods section and P1, P12 and P20 correspond to the a section.

8-OHdG formation.[46,47] This may be explained by the fact that this mutagenic process is strongly inhibited by a DNA repair enzyme, Mutyh.[48] Here we may propose a mechanism in which certain oxidative modification to guanine/cytosine may cause abnormal pairing with the same corresponding base. Recently, it was reported that formamidopyrimidine (FaPy)-guanine, another oxidative DNA base modification,[49,50] would not be responsible for this type of mutation.[51] We suspect that 5,6-dihydroxyuracil and 5-hydroxycytosine which are increased in this model[17] or other aldehyde-modified bases than acrolein-dA are among the possible candidates.

When we reviewed the spectrum of point mutation observed in the *p53*, *tsc2*, *p15*, *p16 and tbp-2* tumor suppressor genes of Fe-NTA-induced rat renal carcinoma, we observed no G:C to C:G transversions, but G:C to T:A (*p53*, *tbp-2*),[16,24] T:A to C:G (*tsc2*), G:C to A:T (*p15 and p16*, *tbp-2*),[21] A:T to T:A (*tbp-2*)[24] and one nucleotide insertion/deletion at repeat sequences (*p16*, *tbp-2*)[21,24] were observed despite the limited available data. There are at least several possibilities to explain this: (i) we have not yet identified the target genes with G:C to C:G mutations; (ii) there are some species-differences between mice and rats; (iii) this mutation spectrum detected in this *gpt* transgenic system is largely reflected in non-geneic genome areas; and (iv) the last possibilities are that G:C to C:G mutations are preferentially repaired by mismatch repair enzyme(s) in non-transgene areas or abundant mutations of this kind lead to lethal effects, affecting fundamental transcriptional activity in the expressed genes. Regarding species differences, another study using the *gpt* delta transgenic rat[52] would answer the question. The data obtained with DnaIP is of note in that 8-OHdG and acrolein-dA were increased in some non-geneic regions after three weeks of repeated administration of Fe-NTA, warranting further studies.

In conclusion, we used the *gpt* delta transgenic mice to evaluate the mutation spectrum of the Fenton reaction-based oxidative renal tubular injury, and found that the major mutations consist of large-size deletions with short homologous sequences at the junctions and transversion-type point mutations at G:C base pairs. The mutant frequency was the highest at the first week of repeated Fe-NTA administration, as shown by the immunohistochemistry of 8-OHdG and acrolein-dA as well as the presence of these two modified bases at the *gpt* loci, indicating that this early stage is one of the critical periods in this Fenton reaction-induced carcinogenesis.

Acknowledgments

This work was supported in part by a Grant-in-Aid from the Ministry of Education, Culture, Sports, Science and Technology of Japan, a Grant-in-Aid for Cancer Research from the Ministry of Health, Labour and Welfare of Japan, and a grant of Long-range Research Initiative (LRI) by Japan Chemical Industry Association (JCIA).

Table 2. Comparison of mutations induced by various mutagens in *gpt* delta transgenic mice

Target	Kidney†				Bone marrow[38]		Colon[39]	
	Control (MF = 1.0)	Fe-NTA-1 W (MF = 2.4)	Fe-NTA-2 W (MF = 1.4)	Fe-NTA-3 W (MF = 1.1)	Control (MF = 1.0)	PhIP (MF = 10.9)	Control (MF = 1.0)	ENU (MF = 3.2)
G:C–A:T	40%	28.6% (1.72)	8.7% (0.30)	16.7% (0.46)	43.1%	14.1%	26.9%	28.3%
A:T–G:C	10%	7.1% (1.70)	21.7% (3.04)	5.6% (0.62)	11.1%	0.0%	3.8%	20.0%
G:C–T:A	10%	10.7% (2.57)	8.7% (1.21)	0% (0.00)	26.4%	52.5%	11.5%	15.0%
G:C–C:G	10%	32.1% (7.70)	4.3% (0.60)	22.2% (2.44)	0.0%	13.1%	7.7%	0.0%
A:T–T:A	0%	3.6% (∞)	4.3% (∞)	11.1% (∞)	5.6%	1.0%	3.8%	28.3%
A:T–C:G	10%	7.1% (1.70)	17.4% (2.44)	11.1% (0.62)	4.2%	0.0%	0.0%	5.0%
Deletion	10%	7.1% (1.70)	26.1% (3.65)	22.2% (2.44)	4.2%	15.1%	38.5%	3.3%
Insertion	10%	3.6% (0.86)	4.3% (0.60)	11.1% (1.22)	5.6%	1.0%	7.7%	0.0%
Others	0%	0.0% (NA)	4.3% (∞)	0.0% (NA)	0.0%	3.0%	0.0%	0.0%

Target	Bone marrow[41]		Liver[53]		Liver[54]		Epidermis[55]		Liver[56]	
	Control (MF = 1.0)	MCC (MF = 2.9)	Control (MF = 1.0)	APNH (MF = 10.3)	Control (MF = 1.0)	γ-ray (MF = 3.2)	Control (MF = 1.0)	UVB (MF = 7.7)	Control (MF = 1.0)	MeIQx (MF = 8.6)
G:C–A:T	24.1%	13.3%	41%	23%	27%	20%	64%	87%	43%	16%
A:T–G:C	3.4%	6.7%	10%	1%	15%	0%	0%	3%	8%	0%
G:C–T:A	31.0%	26.7%	14%	51%	12%	25%	9%	0%	10%	54%
G:C–C:G	10.3%	6.7%	2%	1%	4%	0%	0%	1%	4%	5%
A:T–T:A	6.9%	3.3%	8%	0%	4%	0%	9%	4%	8%	3%
A:T–C:G	10.3%	3.3%	4%	0%	23%	10%	10%	0%	2%	0%
Deletion	13.8%	6.7%	18%	16%	12%	35%	18%	0%	12%	16%
Insertion	0.0%	0.0%	2%	0%	4%	10%	0%	0%	2%	0%
Others	0.0%	33.3%	2%	7%	0%	0%	0%	5%	11%	6%

†present study. The number in parenthesis is the relative mutation frequency in comparison to the untreated control. MF, mutation frequency; NA, not applied; W, week(s); Fe-NTA, ferric nitrilotriacetate; PhIP, 2-amino-1-methyl-6-phenylimidazo [4,5-b]pyridine; ENU, ethylnitrosourea; MMC, mitomycin C; APNH, aminophenylnorharman; UVB, ultraviolet B; MeIQx, 2-amino-3,8-dimethylimidazo[4,5-f]quinoxaline.

References

1 Halliwell B, Gutteridge JMC. *Free radicals in biology and medicine*. Oxford: Clarendon Press, 1999.
2 Iuchi K, Ichimiya A, Akashi A *et al.* Non-Hodgkin's lymphoma of the pleural cavity developing from long-standing pyothorax. *Cancer* 1987; **60**: 1771–5.
3 Gilmour P, Brown D, Beswick P, MacNee W, Rahman I, Donaldson K. Free radical activity of industrial fibers: role of iron in oxidative stress and activation of transcription factors. *Environ Health Perspect* 1997; **105** (Suppl 5): 1313–17.
4 Hodgson J, Darnton A. The quantitative risks of mesothelioma and lung cancer in relation to asbestos exposure. *Ann Occup Hyg* 2000; **44**: 565–601.
5 Uemura N, Okamoto S, Yamamoto S *et al. Helicobacter pylori* infection and the development of gastric cancer. *N Engl J Med* 2001; **345**: 784–9.
6 Naito Y, Yoshikawa T. Carcinogenesis and chemoprevention in gastric cancer associated with *helicobacter pylori* infection: role of oxidants and antioxidants. *J Clin Biochem Nutr* 2005; **36**: 37–49.
7 Collins R, Feldman M, Fordtran J. Colon cancer, dysplasia, and surveillance in patients with ulcerative colitis. A critical review. *N Engl J Med* 1987; **316**: 1654–8.
8 Eaden J, Abrams K, Mayberry J. The risk of colorectal cancer in ulcerative colitis: a meta-analysis. *Gut* 2001; **48**: 526–35.
9 Toyokuni S. Iron-induced carcinogenesis: the role of redox regulation. *Free Radic Biol Med* 1996; **20**: 553–66.
10 Elmberg M, Hultcrantz R, Ekbom A *et al.* Cancer risk in patients with hereditary hemochromatosis and in their first-degree relatives. *Gastroenterology* 2003; **125**: 1733–41.
11 Grodstein F, Speizer F, Hunter D. A prospective study of incident squamous cell carcinoma of the skin in the nurses' health study. *J Natl Cancer Inst* 1995; **87**: 1061–6.
12 Nishigori C, Hattori Y, Toyokuni S. Role of reactive oxygen species in skin carcinogenesis. *Antioxid Redox Signal* 2004; **6**: 561–70.
13 Preston D, Kusumi S, Tomonaga M *et al.* Cancer incidence in atomic bomb survivors. Part III. Leukemia, lymphoma and multiple myeloma, 1950–87. *Radiat Res* 1994; **137**: S68–97.
14 Li JL, Okada S, Hamazaki S, Ebina Y, Midorikawa O. Subacute nephrotoxicity and induction of renal cell carcinoma in mice treated with ferric nitrilotriacetate. *Cancer Res* 1987; **47**: 1867–9.
15 Ebina Y, Okada S, Hamazaki S, Ogino F, Li JL, Midorikawa O. Nephrotoxicity and renal cell carcinoma after use of iron- and aluminum-nitrilotriacetate complexes in rats. *J Natl Cancer Inst* 1986; **76**: 107–13.
16 Nishiyama Y, Suwa H, Okamoto K, Fukumoto M, Hiai H, Toyokuni S. Low incidence of point mutations in *H-*, *K-* and *N-ras* oncogenes and *p53* tumor suppressor gene in renal cell carcinoma and peritoneal mesothelioma of Wistar rats induced by ferric nitrilotriacetate. *Jpn J Cancer Res* 1995; **86**: 1150–8.
17 Toyokuni S, Mori T, Dizdaroglu M. DNA base modifications in renal chromatin of Wistar rats treated with a renal carcinogen, ferric nitrilotriacetate. *Int J Cancer* 1994; **57**: 123–8.
18 Toyokuni S, Uchida K, Okamoto K, Hattori-Nakakuki Y, Hiai H, Stadtman ER. Formation of 4-hydroxy-2-nonenal-modified proteins in the renal proximal tubules of rats treated with a renal carcinogen, ferric nitrilotriacetate. *Proc Natl Acad Sci USA* 1994; **91**: 2616–20.
19 Toyokuni S, Luo XP, Tanaka T, Uchida K, Hiai H, Lehotay DC. Induction of a wide range of C_{2-12} aldehydes and C_{7-12} acyloins in the kidney of Wistar rats after treatment with a renal carcinogen, ferric nitrilotriacetate. *Free Radic Biol Med* 1997; **22**: 1019–27.
20 Zhang D, Okada S, Yu Y, Zheng P, Yamaguchi R, Kasai H. Vitamin E inhibits apoptosis, DNA modification, and cancer incidence induced by iron-mediated peroxidation in Wistar rat kidney. *Cancer Res* 1997; **57**: 2410–14.
21 Tanaka T, Iwasa Y, Kondo S, Hiai H, Toyokuni S. High incidence of allelic loss on chromosome 5 and inactivation of $p15^{INK4B}$ and $p16^{INK4A}$ tumor suppressor genes in oxystress-induced renal cell carcinoma of rats. *Oncogene* 1999; **18**: 3793–7.
22 Hiroyasu M, Ozeki M, Kohda H *et al.* Specific allelic loss of $p16^{INK4A}$ tumor suppressor gene after weeks of iron-mediated oxidative damage during rat renal carcinogenesis. *Am J Pathol* 2002; **160**: 419–24.
23 Tanaka T, Akatsuka S, Ozeki M, Shirase T, Hiai H, Toyokuni S. Redox regulation of annexin 2 and its implications for oxidative stess-induced renal carcinogenesis and metastasis. *Oncogene* 2004; **23**: 3980–9.
24 Dutta KKN, Ishinaka Y, Masutani H *et al.* Thioredoxin-binding protein-2 is a target gene in oxidative stress-induced renal carcinogenesis. *Lab Invest* 2005; **85**: 798–807.
25 Nakatsuka S, Tanaka H, Namba M. Mutagenic effects of ferric nitrilotriacetate (Fe-NTA) on V79 Chinese hamster cells and its inhibitory effects on cell-cell communication. *Carcinogenesis* 1990; **11**: 257–60.

doi: 10.1111/j.1349-7006.2006.00301.x

26 Toyokuni S, Sagripanti JL, Hitchins VM. Cytotoxic and mutagenic effects of ferric nitrilotriacetate on L5178Y mouse lymphoma cells. *Cancer Lett* 1995; **88**: 157–62.
27 Gossen J, de Leeuw W, Tan C *et al.* Efficient rescue of integrated shuttle vectors from transgenic mice: a model for studying mutations in vivo. *Proc Natl Acad Sci USA* 1989; **86**: 7971–5.
28 Kohler S, Provost G, Fieck A *et al.* Spectra of spontaneous and mutagen-induced mutations in the *lacI* gene in transgenic mice. *Proc Natl Acad Sci USA* 1991; **88**: 7958–62.
29 Gondo Y, Shioyama Y, Nakao K, Katsuki M. A novel positive detection system of in vivo mutations in *rpsL* (*strA*) transgenic mice. *Mutat Res* 1996; **360**: 1–14.
30 Nohmi T, Katoh M, Suzuki H *et al.* A new transgenic mouse mutagenesis test system using Spi$^-$ and 6-thioguanine selections. *Environ Mol Mutagen* 1996; **28**: 465–70.
31 Nohmi T, Masumura K. Molecular nature of intrachromosomal deletions and base substitutions induced by environmental mutagens. *Environ Mol Mutagen* 2005; **45**: 150–61.
32 Toyokuni S, Tanaka T, Hattori Y *et al.* Quantitative immunohistochemical determination of 8-hydroxy-2′-deoxyguanosine by a monoclonal antibody N45.1: its application to ferric nitrilotriacetate-induced renal carcinogenesis model. *Lab Invest* 1997; **76**: 365–74.
33 Kawai Y, Furuhata A, Toyokuni S, Aratani Y, Uchida K. Formation of acrolein-derived 2′-deoxyadenosine adduct in an iron-induced carcinogenesis model. *J Biol Chem* 2003; **278**: 50 346–54.
34 Toyokuni S, Akatsuka S, Aung TT, Dutta KK. Free radical-induced carcinogenesis: target genes and fragile genome sites. *Free Radic Res* 2005; **39** (Suppl 1): S30.
35 Akatsuka S, Aung TT, Dutta KK *et al.* Contrasting genome-wide distribution of 8-hydroxyguanine and acrolein-modified adenine during oxidative stress-induced renal carcinogenesis. *Am J Pathol* 2006, in press.
36 Nakae D, Mizumoto Y, Kobayashi E, Noguchi O, Konishi Y. Improved genomic/nuclear DNA extraction for 8-hydroxydeoxyguanosine analysis of small amounts of rat liver tissue. *Cancer Lett* 1995; **97**: 233–9.
37 Ono T, Miyamura Y, Ikehata H *et al.* Spontaneous mutant frequency of *lacZ* gene in spleen of transgenic mouse increases with age. *Mutat Res* 1995; **338**: 183–8.
38 Masumura K, Matsui K, Yamada M *et al.* Mutagenicity of 2-amino-1-methyl-6-phenylimidazo [4,5-b]pyridine (PhIP) in the new *gpt* delta transgenic mouse. *Cancer Lett* 1999; **143**: 241–4.
39 Masumura K, Matsui M, Katoh M *et al.* Spectra of *gpt* mutations in ethylnitrosourea-treated and untreated transgenic mice. *Environ Mol Mutagen* 1999; **34**: 1–8.
40 Nohmi T, Suzuki T, Masumura K. Recent advances in the protocols of transgenic mouse mutation assays. *Mutat Res* 2000; **455**: 191–215.
41 Takeiri A, Mishima M, Tanaka K *et al.* Molecular characterization of mitomycin C-induced large deletions and tandem-base substitutions in the bone marrow of *gpt* delta transgenic mice. *Chem Res Toxicol* 2003; **16**: 171–9.
42 Cariello N, Piegorsch W, Adams W, Skopek T. Computer program for the analysis of mutational spectra: application to *p53* mutations. *Carcinogenesis* 1994; **15**: 2281–5.
43 Shibata A, Masutani M, Kamada N *et al.* Efficient method for mapping and characterizing structures of deletion mutations in *gpt* delta mice using Southern blot analysis with oligo DNA probes. *Environ Mol Mutagen* 2004; **43**: 204–7.
44 Hamazaki S, Okada S, Ebina Y, Midorikawa O. Acute renal failure and glucosuria induced by ferric nitrilotriacetate in rats. *Toxicol Appl Pharmacol* 1985; **77**: 267–74.
45 Toyokuni S, Akatsuka S. What has been learned from the studies of oxidative stress-induced carcinogenesis: proposal of the concept of oxygenomics. *J Clin Biochem Nutr* 2006; **39**: 3–10.
46 Shibutani S, Takeshita M, Grollman AP. Insertion of specific bases during DNA synthesis past the oxidation-damaged base 8-oxodG. *Nature* 1991; **349**: 431–4.
47 Kasai H. Analysis of a form of oxidative DNA damage, 8-hydroxy-2′-deoxyguanosine, as a marker of cellular oxidative stress during carcinogenesis. *Mutat Res* 1997; **387**: 147–63.
48 Nakabeppu Y. Regulation of intracellular localization of human MTH1, OGG1, and MYH proteins for repair of oxidative DNA damage. *Prog Nucl Acid Res Mol Biol* 2001; **68**: 75–94.
49 Steenken S. Purine bases, nucleosides, and nucleotides: aqueous solution redox chemistry and transformation reactions of their radical reactions and e$^-$ and. OH adducts. *Chem Rev* 1989; **89**: 503–20.
50 Dizdaroglu M. Chemical determination of free radical-induced damage to DNA. *Free Radic Biol Med* 1991; **10**: 225–42.
51 Ober M, Muller H, Pieck C, Gierlich J, Carell T. Base pairing and replicative processing of the formamidopyrimidine-dG DNA lesion. *J Am Chem Soc* 2005; **127**: 18 143–9.
52 Hayashi H, Kondo H, Masumura K, Shindo Y, Nohmi T. Novel transgenic rat for *in vivo* genotoxicity assays using 6-thioguanine and Spi$^-$ selection. *Environ Mol Mutagen* 2003; **41**: 253–9.
53 Masumura K, Totsuka Y, Wakabayashi K, Nohmi T. Potent genotoxicity of aminophenylnorharman, formed from non-mutagenic norharman and aniline, in the liver of *gpt* delta transgenic mouse. *Carcinogenesis* 2003; **24**: 1985–93.
54 Masumura K, Kuniya K, Kurobe T, Fukuoka M, Yatagai F, Nohmi T. Heavy-ion-induced mutations in the *gpt* delta transgenic mouse: comparison of mutation spectra induced by heavy-ion, X-ray, and gamma-ray radiation. *Environ Mol Mutagen* 2002; **40**: 207–15.
55 Horiguchi M, Masumura K, Ikehata H *et al.* UVB-induced *gpt* mutations in the skin of *gpt* delta transgenic mice. *Environ Mol Mutagen* 1999; **34**: 72–9.
56 Masumura K, Horiguchi M, Nishikawa A *et al.* Low dose genotoxicity of 2-amino-3,8-dimethylimidazo[4,5-f]quinoxaline (MeIQx) in *gpt* delta transgenic mice. *Mutat Res* 2003; **541**: 91–102.

Available online at www.sciencedirect.com
ScienceDirect
ELSEVIER
Mutation Research 609 (2006) 102–115
Genetic Toxicology and Environmental Mutagenesis
www.elsevier.com/locate/gentox
Community address: www.elsevier.com/locate/mutres

A newly established GDL1 cell line from *gpt* delta mice well reflects the in vivo mutation spectra induced by mitomycin C

Akira Takeiri [a,*], Masayuki Mishima [a], Kenji Tanaka [a], Akifumi Shioda [a], Asako Harada [a], Kazuto Watanabe [a], Ken-Ichi Masumura [b], Takehiko Nohmi [b]

[a] *Fuji Gotemba Research Laboratories, Chugai Pharmaceutical Co. Ltd., 1-135 Komakado, Gotemba, Shizuoka 412-8513, Japan*
[b] *Division of Genetics and Mutagenesis, National Institute of Health Sciences, 1-18-1 Kamiyoga, Setagaya, Tokyo 158-8501, Japan*

Received 8 May 2006; received in revised form 19 June 2006; accepted 30 June 2006
Available online 17 August 2006

Abstract

In order to create a novel in vitro test system for detection of large deletions and point mutations, we developed an immortalized cell line. A SV40 large T antigen expression unit was introduced into fibroblasts derived from *gpt* delta mouse lung tissue and a selected clone was established as the *gpt* delta L1 (GDL1) cell line. The novel GDL1 cells were examined for mutant frequencies (MFs) and for molecular characterization of mutations induced by mitomycin C (MMC). The GDL1 cells were treated with MMC at doses of 0.025, 0.05, and 0.1 μg/mL for 24 h and mutations were detected by Spi$^-$ and 6-thioguanine (6-TG) selections. The MFs of the MMC-treated cells increased up to 3.4-fold with Spi$^-$ selection and 3.5-fold with 6-TG selection compared to MFs of untreated cells. In the Spi$^-$ mutants, the number of large (up to 76 kilo base pair (kbp)) deletion mutations increased. A majority of the large deletion mutations had 1–4 base pairs (bp) of microhomology in the deletion junctions. A number of the rearranged deletion mutations were accompanied with deletions and insertions of up to 1.1 kbp. In the *gpt* mutants obtained from 6-TG selection, single base substitutions of G:C to T:A, tandem base substitutions occurring at the 5′-GG-3′ or 5′-CG-3′ sequence, and deletion mutations larger than 2 bp were increased. We compared the spectrum of MMC-induced mutations observed in vitro to that of in vivo using *gpt* delta mice, which we reported previously. Although a slight difference was observed in MMC-induced mutation spectra between in vitro and in vivo, the mutations detected in vitro included all of the types of mutations observed in vivo. The present study demonstrates that the newly established GDL1 cell line is a useful tool to detect and analyze various mutations including large deletions in mammalian cells.

Keywords: Mitomycin C; Cell line; *gpt* delta mice

1. Introduction

Point mutations and deletion mutations are major genotoxic events induced by chemicals and ionizing radiation. In particular, deletion mutations constitute an important class of mutations that may result in a variety of human diseases including cancer [1]. Development of various in vivo test systems suitable for detection and analysis of point mutations have provided a better understanding of molecular properties of chemical mutagenesis [2,3]. However, fewer methodologies are available to analyze deletion mutations compared with

* Corresponding author. Tel.: +81 550 87 6376; fax: +81 550 87 6383.
E-mail address: takeiriakr@chugai-pharm.co.jp (A. Takeiri).

1383-5718/$ – see front matter © 2006 Elsevier B.V. All rights reserved.
doi:10.1016/j.mrgentox.2006.06.026

point mutations. Recently, successful and convenient approaches for the analysis of deletion mutations using transgenic (TG) animal models have been constructed [4,5]. The *lacZ* plasmid-based TG mouse assay detects deletion mutations induced by X-ray and cisplatin [5,6]. The *gpt* delta mice efficiently detects deletion mutations induced by various mutagens, e.g., mitomycin C (MMC) [7,8], heavy-ion, X-ray [9], gamma-ray [9,10], and ultraviolet B [11,12]. In the *gpt* delta mice, approximately 80 copies of the lambda EG10 shuttle vector DNA carrying the *red/gam* genes of lambda phage and the *gpt* gene of *Escherichia coli* are integrated into this TG mouse on chromosome 17 of the C57BL/6J background [2,4]. Deletion mutations in the *red/gam* genes and point mutations in the *gpt* gene can be individually identified by Spi^- (sensitive to P2 interference) selection and 6-thioguanine (6-TG) selection, respectively [2].

MMC is a natural cytotoxic and genotoxic agent used in clinical anticancer chemotherapy [13]. The mode of action of this agent in mutagenicity is intriguing and well investigated. MMC alkylates DNA in several different ways [14]. It binds to the N^2 position of guanine in DNA and forms monoalkylation products. Furthermore, after the carbamate at C-10″ is lost, it will give rise to another active site capable of alkylating the second guanine within the DNA. Alkylation of two guanine bases on the same DNA strand results in the formation of intrastrand cross-links within the 5′-GG-3′ sequence, and the alkylation of guanine bases on opposite DNA strands leads to the formation of interstrand cross-links within the 5′-CG-3′ sequence [15–19]. Interaction of MMC and DNA strands causes the production of characteristic mutations. In our previous in vivo study, MMC-induced tandem base substitutions and deletion mutations up to about 8 kilo base pair (kbp) in size [8].

Since it is often advantageous to use in vitro test systems in mechanistic investigations, we newly established the GDL1 cell line harboring the same reporter gene system as *gpt* delta mice. The cells were established from lung fibroblasts of the *gpt* delta mice with a functional reduction of p53 protein by intracellular expression of the Simian virus 40 large T antigen (SV40 T antigen). GDL1 was exposed to MMC to characterize the induced mutations. Comparing the results from GDL1 cells with those previously reported in vivo, there was little difference in mutation spectra and all of the types of mutations in vivo were involved in the events detected with GDL1 cells. The GDL1 cell is a novel tool available for molecular analysis of deletion mutations. Furthermore, we here discuss the contribution of the dysfunction of p53 by the SV40 T antigen to the differences between the MMC-induced mutations in the GDL1 cells and in the *gpt* delta mice.

2. Materials and methods

2.1. Collection of the fibroblasts

Lung tissues were obtained from 21-week-old female *gpt* delta mice maintained in our laboratory. The tissues were minced in Eagle's minimum essential medium (MEM, Sigma–Aldrich, St. Louis, MO, USA) and trypsinized in MEM including 0.1% (w/v) trypsin, 0.01% (w/v) EDTA for 1 h at 37 °C. After centrifugation, the down pellet containing fibroblast cells was suspended in Dulbecco's modified Eagle's medium (DMEM, Sigma–Aldrich, St. Louis, MO, USA) including 10% (v/v) fetal bovine serum (FBS, Invitrogen, Carlsbad, CA, USA). The cells were cultured in 75-cm^2 culture flasks (BD Biosciences, Franklin Lakes, NJ, USA) in an atmosphere of 5% CO_2 at 37 °C.

2.2. Establishment of the cell line

A plasmid encoding the complete sequence for the SV40 T antigen was obtained from the Health Science Research Resources Bank (Osaka, Japan): pMTIOD, registration no. VG026 [20]. The complete sequence of the T antigen gene was excised from pMTIOD and inserted into an expression vector at the downstream of the elongation factor 1 alpha promoter, resulting in pCOSV1. The constructed vector was introduced into the fibroblasts using a lipofection reagent, FuGENE6 (Roche Diagnostics, Tokyo, Japan). The transfectants were selected by culture in DMEM containing 100 μg/mL of G-418 for 1 week. The cells were cloned and, after approximately 60 passages in DMEM supplemented with 10% (v/v) FBS in an atmosphere of 5% CO_2 at 37 °C, we selected a stably growing single clone (clone #2) to establish the GDL1 cell.

2.3. Measurement of chromosome number and immunostaining

A single cloned GDL1 cell stock frozen in liquid nitrogen was thawed and maintained in DMEM supplemented with 10% (v/v) FBS in an atmosphere of 5% CO_2 at 37 °C. For measurement of chromosome number, the cells were treated with 0.1 μg/mL colcemid (Wako Pure Chemical Industries, Osaka, Japan) for 2 h. The trypsinized cells using PBS including 0.1% (w/v) trypsin, 0.01% (w/v) EDTA were suspended in 75 mM KCl hypotonic solution and fixed with acetic acid and methanol (1:3) mixture. The cell suspensions were dropped on glass slides and dried. The metaphase spreads of the cells were stained with Giemsa and each chromosome of 100 metaphases was scored. The cells cultured in a 24-well culture plate (BD Biosciences, Franklin Lakes, NJ, USA) were fixed by 99.5% methanol and then examined for SV40 T antigen expression by immunofluorescent assay. The cells were stained with anti-

SV40 large T monoclonal antibody, SV40T-Ag (Ab-2) (EMD Biosciences, San Diego, CA, USA), and FITC conjugated anti-mouse immunoglobulin polyclonal antibody (Dako Cytomation, Carpinteria, CA, USA).

2.4. Cytotoxicity

GDL1 cells were seeded in 12-multiwell culture plate (Corning, Corning, NY, USA) at a density of 4×10^4 cells/mL in each well. One day after the seeding, the cells were treated with mitomycin C (MMC, CAS no. 50-07-7, Kyowa Hakko Kogyo, Tokyo, Japan) at doses of 0.025, 0.05, and 0.1 μg/mL for 24 h. The solutions of chemicals were freshly prepared at 100-fold of final concentration in saline. The cells were trypsinized and resuspended in DMEM supplemented with 10% (v/v) FBS. The number of cells was counted using automated hematology analyzer KX-21 (Sysmex, Kobe, Japan).

2.5. Treatment with MMC and preparation of lambda EG10 phage

GDL1 cells were subcultured and divided into flasks for chemical treatment at 1×10^5 cells/5 mL medium per 25-cm^2 culture flask 2 days before the treatment. Three culture flasks were prepared for each dose of MMC and untreated control. The cells were exposed to MMC at doses of 0.025, 0.05, or 0.1 μg/mL for 24 h, washed, and cultured for an additional 6 days. The additional 6 days is considered sufficient for fixation of mutations [21]. During the 6-day culture, the cells were subcultured two times; the culture volume was increased to 10 mL and transferred to 75-cm^2 culture flasks. DNA samples of the cells were prepared using a RecoverEase DNA isolation kit (Stratagene, La Jolla, CA, USA). The lambda EG10 phages were rescued from the DNA by in vitro packaging reaction using Transpack packaging extract (Stratagene, La Jolla, CA, USA) according to the manufacturer's instruction.

2.6. Measurement of mutant frequency (MF) and sequence analysis

The Spi$^-$ mutation assay was performed as described previously [2,10,12]. The rescued phages were infected to *E. coli* XL1-Blue MRA (P2) (Stratagene, La Jolla, CA, USA). The infected host cells were poured onto lambda-trypticase agar plates and incubated at 37 °C to detect mutant phage plaque. The rescued phages were diluted and infected to *E. coli* XL1-Blue MRA (Stratagene, La Jolla, CA, USA) to determine total number of phage plaques. The Spi$^-$ MF was calculated as previously reported [2,10,12]. The entire sequence of lambda EG10 phage and the detail method of Spi$^-$ selection and 6-TG selection is available at: http://www.dgm2alpha.nihs.go.jp/dgm2/.

The *gpt* mutagenesis assay was performed according to previous method [2,11]. Briefly, the lambda EG10 phages were converted to plasmids by the infection to *E. coli* YG6020 which was expressing Cre recombinase. The infected bacteria were poured onto agar plates containing chloramphenicol (Cm) and 6-TG. The plates were incubated at 37 °C for the selection of colonies harboring plasmids carrying the mutated *gpt* gene. The infected host bacteria were diluted and poured on the plates containing Cm alone to determine the total number of rescued plasmids. The *gpt* MF was calculated as previously reported [2,11].

In the cells treated with 0.1 μg/mL MMC or untreated, the Spi$^-$ mutants and *gpt* mutants obtained from Spi$^-$ selection and 6-TG selection, respectively, were used for sequence analysis as previously described [2,8,10–12]. The sequences of the *gam* gene or DNA sequences surrounding the deletion junction were analyzed in 43 Spi$^-$ mutants from untreated cells and 45 mutants from MMC-treated cells. Forty-five *gpt* mutants each from untreated and MMC-treated cells were analyzed. In Spi$^-$ mutants and *gpt* mutants, the mutations analyzed were classified by the types of mutation. The ratio of each type of mutation to total mutation was multiplied by total MF for calculation of specific MF. The specific MFs of the MMC-treated cells were statistically compared to those of the control cells using Fisher's exact test according to the method of Carr and Gorelick [22].

3. Results

3.1. Induction of Spi$^-$ and gpt mutations by MMC in GDL1 cells

We established the GDL1 cell line from fibroblasts of the lung of *gpt* delta TG mice by introduction of plasmid pCOSV1 expressing SV40 T antigen. The doubling time of the cell line was approximately 12 h (data not shown), and the cells were polyploid with a modal chromosome number of 74 ($2N = 40$ in mice) (Fig. 1). SV40 T antigen was expressed and localized in the nucleus (data not shown). To characterize the GDL1 cell line as a tester for genotoxicity assays, we examined the Spi$^-$ and *gpt* mutations induced by MMC at the molecular

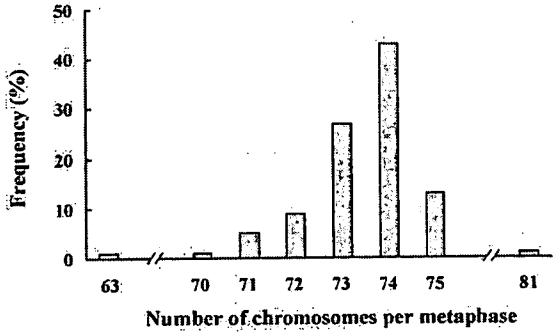

Fig. 1. Chromosome frequency distribution in GDL1 cells. The number of chromosomes in a spread of 100 metaphase cells was calculated. The modal chromosome number was 74 ($2N = 40$ in mice).

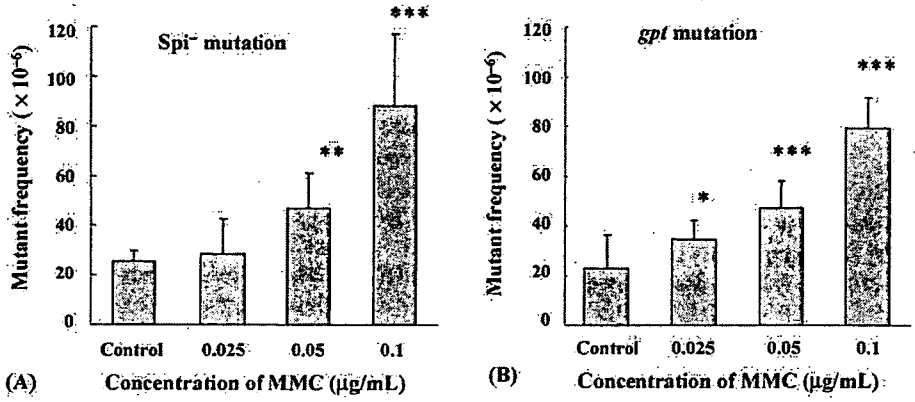

Fig. 2. Mutant frequencies in MMC-treated GDL1 cells. (A) Spi⁻ mutant frequencies; (B) *gpt* mutant frequencies. Cells were treated with MMC at the doses of 0.025, 0.05, and 0.1 μg/mL for 24 h. After a 6-day culture, the cells were harvested. As the control, untreated cells were collected after a 6-day cell culture. Spi⁻ mutant frequency in Spi⁻ selection and *gpt* mutant frequency in 6-TG selection were determined. *P* values calculated by Fisher's exact test were $P < 0.05$ (*), $P < 0.001$ (**), and $P < 0.0001$ (***). Bars represent mean and standard deviations of data obtained from three independent cell culture flasks.

level. In the MMC-treated group, Spi⁻ MFs at concentrations of 0.025, 0.05, and 0.1 μg/mL were 28.4×10^{-6}, 47.0×10^{-6}, and 88.0×10^{-6}, respectively (Fig. 2A). MFs increased in a dose-dependent manner up to 3.4 times higher than the control group, i.e., 25.6×10^{-6}. On the other hand, *gpt* MFs at concentrations of 0.025, 0.05, and 0.1 μg/mL were 34.8×10^{-6}, 47.0×10^{-6}, and 78.9×10^{-6}, respectively (Fig. 2B). The *gpt* MFs increased in a dose-dependent manner up to 3.5-fold compared with the control group, i.e., 22.7×10^{-6}. The numbers of cells treated with MMC for 24 h were 73, 53, and 40% of untreated cells in 0.025, 0.05, and 0.1 μg/mL of MMC, respectively.

3.2. Molecular nature of Spi⁻ mutations induced by MMC

To characterize the molecular nature of Spi⁻ mutations induced by MMC, we sequenced 43 and 45 Spi⁻ mutants from untreated cells and cells treated with MMC (0.1 μg/mL), respectively, and categorized them into five classes (Table 1). The specific MF for each class and subclass was determined by multiplying the percentage of each class of mutants and the total MF, and the calculated values were compared between untreated and treated groups.

Large deletions more than 1 kbp in deletion size were classified as class I. They were subclassified into classes I-A and I-B depending on the existence of homologous sequences at the junctions. The specific MF class I-A, i.e., large deletion with short homology (microhomology) at the junction, was enhanced more than four-fold by treatments with MMC (17.6×10^{-6} versus 4.2×10^{-6}, Table 1). The deletion sizes of nine class I-A mutants from the MMC-treated group were from 3829 to 7178 base pair (bp) (Fig. 3). They were all unique in size and position of the deletions. In addition, three class I-B mutants, i.e., large deletions without short homologous sequence, were identified in the treated group. Two of them were simple deletion mutants with deletion sizes of 3345 and 5204 bp, but one mutant, sM2-3, had an insertion of 16 bp with a deletion size of 5676 bp (Fig. 3). In contrast, class I mutants of the untreated group were all class I-A and no class I-B mutants were identified. Five of seven class I-A mutants from untreated cells were completely the same in size and position of deletions (Fig. 3). Since they were independently identified in the mutants and derived from independent culture flasks, they might have been generated by hot spot mutations in untreated GDL1 cells. Alternatively, the mutation might have occurred prior to the subculture of the cells for untreated groups (clonally expanded mutants). The deletion sizes of the seven class I-A mutants were from 3308 to 6827 bp.

Midsized deletions with sizes of from 2 bp to 1 kbp were classified as class II. The specific MF for class II was enhanced more than six times by the treatments with MMC (7.8×10^{-6} versus 1.2×10^{-6}, Table 1). The deletion sizes of four mutants in the MMC-treated group were from 9 to 129 bp (Fig. 3). They were all unique in size and position of the deletions. Two of them were simple deletion mutants with deletion sizes of 9 and 129 bp, and the deleted regions were flanked by two short homologous sequences. Other two deletions had flush ends but had insertions of 9 and 8 bp in the junctions. The deleted sequences were enclosed by short repetitive sequences.

Table 1
Summary of Spi⁻ mutations derived from the GDL1 cells

Type of mutation	Class of mutation	Control		MMC		*P* value[a]
		No. of mutants (%)	Specific MF[b] ($\times 10^{-6}$)	No. of mutants (%)	Specific MF[b] ($\times 10^{-6}$)	
Large deletion (>1 kbp)						
With microhomology	I-A	7 (16.3)	4.2	9 (20.0)	17.6	<0.01
Without microhomology	I-B	0 (0.0)	0.0	3 (6.7)	5.9	<0.05
Midsize deletion (2 bp to 1 kbp)	II	2 (4.7)	1.2	4 (8.9)	7.8	<0.05
Single base deletion						
At run sequence	III-A	29 (67.4)	17.3	17 (37.8)	33.2	0.06
At non-run sequence	III-B	2 (4.7)	1.2	0 (0.0)	0.0	1.00
Complex mutation	IV	0 (0.0)	0.0	5 (11.1)	9.8	<0.001
Miscellaneous mutation	V					
Transversion						
G:C → T:A		2 (4.7)	1.2	0 (0.0)	0.0	1.00
A:T → T:A		0 (0.0)	0.0	2 (4.4)	3.9	0.06
Tandem base substitution						
GG:CC → TA:AT		0 (0.0)	0.0	1 (2.2)	2.0	0.24
GG:CC → TT:AA		0 (0.0)	0.0	1 (2.2)	2.0	0.24
Other substitution		1 (2.3)	0.6	2 (4.4)	3.9	0.15
Unidentified		0 (0.0)	0.0	1 (2.2)	2.0	0.24
Total		43 (100)	25.6	45 (100)	88.0	<0.0001

[a] *P* values were determined using Fisher's exact test according to Carr and Gorelick [22].
[b] Specific MF was calculated by multiplying the total mutation frequency by the ratio of each type of mutation to the total mutation.

In the control group, two of the class II mutations were simple deletions with sizes of 13 and 206 bp.

Single base deletions occurring in the *gam* gene were classified as class III with subclasses of classes III-A and III-B. Single base deletion induced at a run sequence of identical bases, e.g., −1A deletion at 5′-AAAAAA-3′ of nucleotides 295–300 (Fig. 4), were classified as class III-A and single base deletions occurring at a non-run sequence were classified as class III-B. The specific MF of class III-A was enhanced about two times by the MMC treatments (33.2×10^{-6} versus 17.3×10^{-6}, Table 1). The class III-A was dominant over III-B in both MMC-treated and control groups.

Complex mutations were classified as class IV. Five mutants of this class were observed in the MMC-treated group, while no such mutants were observed in the control group. All five MMC-induced class IV mutations were deletions with complex rearrangements (Figs. 3 and 5). Mutant sM1-9, with a deleted region of approximately 5 kbp, had an inserted fragment larger than 1 kbp, which was homologous to the sequence in chromosome 16 of mouse from the DNA data base (http://www.ddbj.nig.ac.jp/). Since the lambda EG10 DNA is integrated in chromosome 17 of the *gpt* delta mouse, the mutation was due to inter-chromosomal translocation. In mutant sM2-6, a 7632 bp region including the *red/gam* genes was deleted, and three DNA fragments derived from the deleted region – fragment 1 (457 bp), fragment 2 (153 bp), and fragment 3 (1115 bp) – were incorrectly inserted again. In mutant sM2-12, a region of 3459 bp was deleted and a fragment of 403 bp, which was located at approximately 1.2 kbp from the deleted site, was inserted into the deletion site. In mutant sM2-14, the deletion size was approximately 5 kbp. A sequence existing approximately 6 kbp away from the deletion site was inserted into the deletion junction in the opposite direction. The accurate size of the inserted fragment was not determined. In mutant sM3-7, the deletion size determined by agarose-gel electrophoresis of the PCR product was approximately 5 kbp. A DNA fragment located approximately 18 kbp away from the deletion site was inserted into the deletion site. The size of the inserted fragment could not be determined accurately. Almost all of the deletion junctions observed in the complex rearrangements mentioned above had microhomology sequences (Fig. 3).

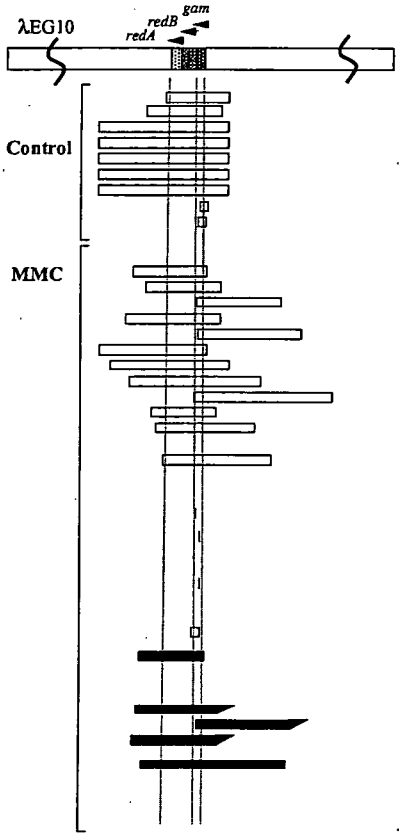

Treatment	Mutant code	Class	Mutation	Sequence of deletion junction
Control	sC3- 3	I-A	-3,308 bp deletion	TTCCTGGTGTTTCTT TCTTCTGTTGAGTTA
	sC2- 1	I-A	-3,979 bp deletion	TTATTGAAAAATAAA TAAACTGGAAAGCAA
	sC1- 8	I-A	-6,827 bp deletion	TTGTTTTTACTGCGGG GATGAATCCGTCAGT
	sC1- 9	I-A	-6,827 bp deletion	TTGTTTTTACTGCGGG GATGAATCCGTCAGT
	sC2- 7	I-A	-6,827 bp deletion	TTGTTTTTCTGCGGG GATGAATCCGTCAGT
	sC3- 9	I-A	-6,827 bp deletion	TTGTTTTTACTGCGGG GATGAATCCGTCAGT
	sC3- 10	I-A	-6,827 bp deletion	TTGTTTTTACTGCGGG GATGAATCCGTCAGT
	sC1- 2	II	-13 bp deletion	CGTCACTACCAGCAG AGAGAAAGAGGCAGA
	sC3- 11	II	-206 bp deletion	CTAATCAGCCCGGCA ACGGGGCCAGCAAAA
MMC 0.1 μg/mL	sM1- 7	I-A	-3,829 bp deletion	GATGTTTCGTGAAGC CGGTGGAAACGATAC
	sM1- 10	I-A	-3,979 bp deletion	TTATTGAAAAATAAA TAAACTGGAAAGCAA
	sM1- 12	I-A	-4,424 bp deletion	TGCAGGATATCGACC ACCATTGCTCACCAC
	sM3- 12	I-A	-4,996 bp deletion	CTACCAAACAATGCC GCCTTGAAACAGTTC
	sM3- 11	I-A	-5,454 bp deletion	ACGCGGCGCTCGATG GATGACGATGTTGAG
	sM2- 9	I-A	-5,618 bp deletion	CTAACCCCCTTTCCT CTTTACTGCCATATT
	sM2- 15	I-A	-6,230 bp deletion	TGCAGGAACCATGAT GATATCTTTATGTCG
	sM3- 15	I-A	-6,823 bp deletion	AGGAACAACTGCCGG GGAGAATGGAATGGA
	sM1- 15	I-A	-7,178 bp deletion	ATGATAACCATTGCG CGTGTCGGCATGGAT
	sM3- 13	I-B	-3,345 bp deletion	AAGGCTTTGGGGTGT ACGCCTGGTCGTTCA
	sM3- 1	I-B	-5,204 bp deletion	GGAGAGATCCCCTGGC GGAGCTACAGGCTCC
	sM2- 3	I-B	-5,676 bp deletion, +16 bp insertion	TTTTTACCGCCAGAT AGCCGCATCCCTTTC ^ AATGGTCTGCGCTTGA
	sM3- 4	II	-9 bp deletion	CATGGCAGAACACAT ATGGTTGAAACCATT
	sM2- 10	II	-13 bp deletion, +9 bp insertion	CACTACCAGCAGCTC ^ CTGAGCCTC AAGAGGCAGAACTGG
	sM3- 9	II	-36 bp deletion, +8 bp insertion	GTCTTGAGGCTCAGA ^ CGATCACT AGAAAGAGGCAGAAC
	sM2- 11	II	-129 bp deletion	AACACATCCGGTACA AACTGATCACCACTC
	sM2- 12	IV	-3,459 bp and -405 bp deletion +403 bp and +28 bp insertion	ATGGCTTGATCGCTA AAATGAAGTGGTCTG GCCACTTTTATTGGC TGGCCAGCAGAGGAA TGCGAAATGAAGTGG GAAAATGCTGAATTT
	sM3- 7	IV	approx. -5 kbp deletion, insertion	AGAATCCAGATGGAT ATCAATGTTGTGCAG
	sM2- 14	IV	approx. -5 kbp deletion, reverse-fragment insertion	AGCCCACAATGCCGC CATCGATCATTTGCA
	sM1- 9	IV	approx. -5 kbp deletion, inter-chromosomal translocation	TTTATTTCCACTTTT CAATATTACATAACA
	sM2- 6	IV	-7,632 bp deletion, +153 bp insertion and two reverse-fragments (+457 bp and +1,115 bp) insertion	CGCCAGCGACGCACG CGCTATTACGGGGTT TCCCTGCCGTTAGCG GCGTCCAGTACGTGG CGGGAGAGCAGGCGG GCGGGTTGTGGACCT CGCAGGCATTACGTG TGTAATTCTTCTATT

Fig. 3. Deletion mutations classified as classes I-A, I-B, II, and IV recovered from MMC-treated and untreated cells. A partial genetic map of the lambda EG10 transgene, including the *gam* and the *redBA* target regions of Spi⁻ selection is shown. Horizontal bars represent regions deleted in Spi⁻ mutants. Open bars represent the deleted regions of classes I-A, I-B, and II mutants, which have no rearrangements. Closed bars show class IV deletions, which have rearrangements within the deleted regions. An angled end of a bar denotes that the deletion positions have not been precisely determined. Junctions are indicated as a space between the left and right sequences. Microhomology sequences in the junctions are underlined. One of two microhomologies in the junctions that are underlined is deleted when the two DNA fragments are joined. (^) The insertion of a sequence in the deletion junction. All the mutants were analyzed with mutant codes. The first letter in the mutant code, 's' stands for Spi⁻ mutants. 'M' stands for MMC-treated group and 'C' for the untreated control group. The third number is the ID number for the independent culture flask. The last number is the mutant ID number. The sM2-3 represents the Spi⁻ mutants ID #3 in the MMC-treated flask #2.

Miscellaneous mutations including base substitutions in the *gam* gene were classified as class V (Table 1). In the MMC-treated group, tandem base substitutions at 5′-GG-3′ were observed.

3.3. Molecular characteristics of gpt mutations induced by MMC

To analyze MMC-induced point mutations, 45 mutations observed in the MMC-treated cells and 46 mutations derived from untreated control cells were identified at the sequence level (Table 2). Specific MFs of single base substitutions of G:C to T:A (substitutions of G to T or substitutions of C to A in Fig. 6) was 6.7-fold higher in the MMC-treated group than in the untreated group (26.3×10^{-6} versus 3.9×10^{-6}, Table 2). In the MMC-treated group, 19 of 26 (73%) single base substitutions was observed in the 5′-CG-3′ or 5′-GG-3′ sequence, in which MMC monoadducts were preferentially induced (Fig. 6) [23,24]. In the control group, 18 of 34 (53%) single base substitutions occurred at the 5′-CG-3′ or 5′-GG-3′ sequence (Fig. 6).

For insertion mutations with an insertion size larger than 2 bp, specific MF was 3.5×10^{-6} in the MMC-treated group, while no such mutations were observed in the control group (Table 2). The two mutations induced by MMC treatment were both 9 bp insertions (Fig. 6). One had a sequence change of 5′-GCGcagaagGCG-3′ to 5′-GCGcagaaggcgcagaagGCG-3′ in nucleotide 229–230 in the *gpt* gene, and the other had 5′-TCCcgccaatcTCC-3′ to 5′-TCCgccaatctccgccaatcTCC-3′ in nucleotide 438–439 (the sequences underlined

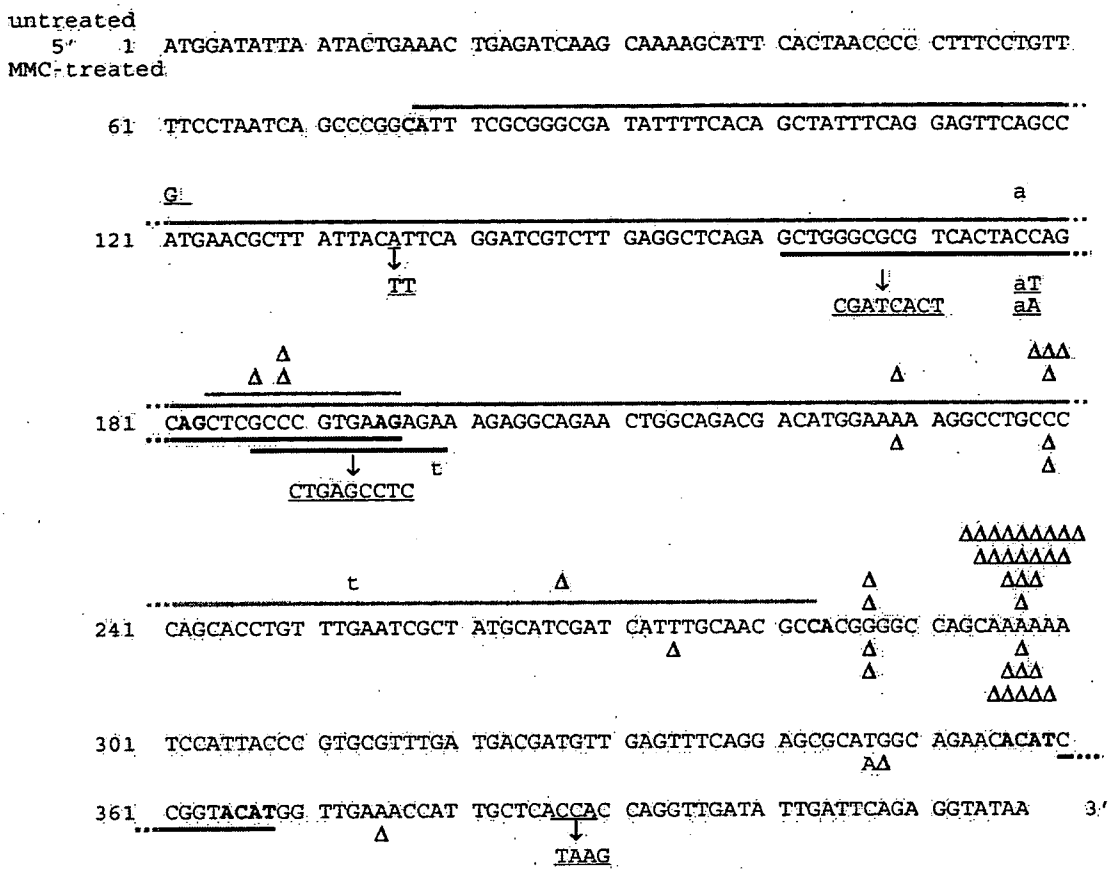

Fig. 4. Spi⁻ mutants of classes II, III-A, III-B, and V in the *gam* gene. The sequence from top to bottom represents the coding region of the *gam* gene. Mutations shown below the strands were detected in MMC-treated cells; those above the strands were observed in untreated cells. (Δ) Single base deletion. Sequence substitutions are underlined, the underlined sequences in the strands were substituted for the underlined sequence represented below the strands. Bars represent a deleted sequence in deletion mutations. The short homologous sequences associated with deletions are represented in bold. Two deletion mutations with sequence substitution in MMC-treated cells were substitutions of 5′-gctgggcgcgtcactaccagcagctcgcccgtgaag-3′ to 5′-cgatcact-3′ and 5′-gcccgtgaagaga-3′ to 5′-ctgagcctc-3′, and were classified as class II. The lowercase letters in the substituted sequences formed stop codon with adjoining two bases.

are altered sequences and the capital letters represent microhomology). In the former and latter mutants, 5′-cagaaggcg-3′ and 5′-cgccaatctc-3′, respectively, were repeated.

In deletion mutations larger than 2 bp, the specific MF in the MMC-treated group was 14 times higher than the untreated group (7.0×10^{-6} versus 0.5×10^{-6}, Table 2). In the MMC-treated group, four such deletions were identified (Fig. 6). They were an 8-bp deletion in 5′-CtcgcaagC-3′ of position 56–63, a 5-bp deletion in 5′-TaccgT-3′ of position 169–173, a 20-bp deletion in 5′-TCgcaaaaccggctggtcgTC-3′ of position 339–358, and a 329-bp deletion in 5′-CACTTcacatg· · ·aaagcgCACTT-3′ of position −3 to 326 in the *gpt* gene (not shown). All these deletions were enclosed by microhomology sequences. In the control group, one deletion with a size of 6 bp in 5′-GGCgaaGGC-3′ of position 241–246 was identified.

The specific MF of tandem base substitutions was 8.8×10^{-6} in the MMC-treated group, whereas no such mutations were observed in the untreated group. All five tandem base substitutions in the MMC-treated cells occurred in the 5′-GG-3′ or 5′-CG-3′ sequence, in which formation of MMC cross-links has been reported [15,16].

The specific MF of "others" was enhanced 14-fold by MMC treatments (7.0×10^{-6} versus 0.5×10^{-6}, Table 2). Four such MMC-induced mutations include a sequence substitution of 5′-TACCG-3′ to 5′-AACTA-3′ in position 122–126, a substitution 5′-CGG-3′ to 5′-AT-3′ in position 347–349, a −565-bp deletion accompanied by +1 bp insertion in position 11–575 (not shown) and a

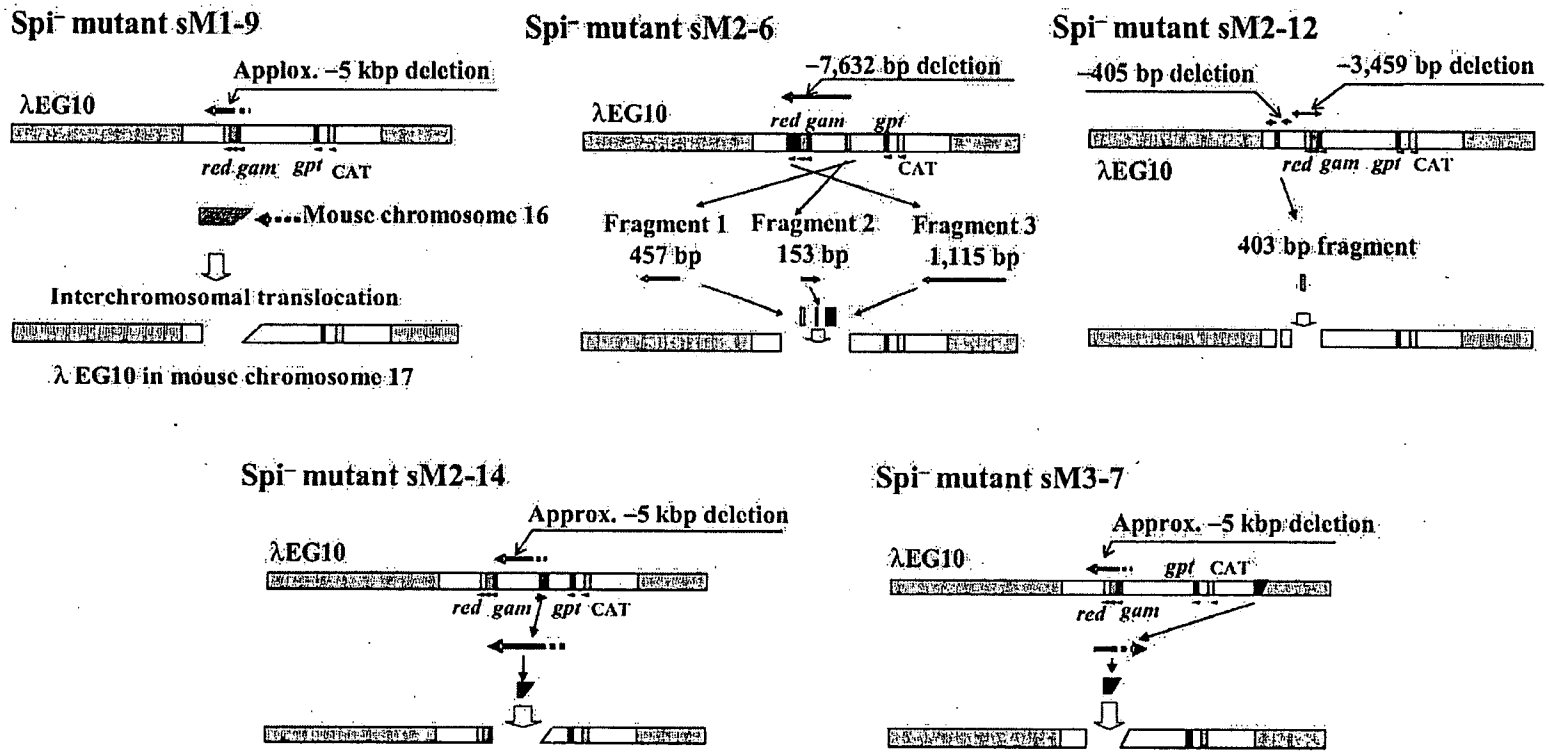

Fig. 5. Rearrangements induced in the Spi⁻ mutants derived from MMC-treated GDL1 cells. Complex deletions with insertions were observed in 5 Spi⁻ mutants. The upper bars in each mutant represent the lambda EG10 gene. The lower bars show mutants that have deletions and insertions resulting from MMC treatment. In the Spi⁻ mutant sM1-9, approximately 5 kbp were deleted. The inserted sequence was not found in the lambda EG10 gene but in chromosome 16 of the mouse genome. In Spi⁻ mutant sM2-6, 7632 bp including the *gam* gene sequence was deleted, and three DNA fragments within the deleted sequence, fragment 1 (457 bp), fragment 2 (153 bp), and fragment 3 (1115 bp), were inserted. The direction and order of the inserted fragments were different from that of the original sequence. In Spi⁻ mutant sM2-12, a fragment of 3459 bp including the *gam* gene was deleted and a fragment of 403 bp was inserted into the deletion site. In Spi⁻ mutant sM2-14, the deletion size was approximately 5 kbp. An inverted sequence existing approximately 6 kbp from the deletion site was inserted into the deletion junction. In Spi⁻ mutant sM3-7, the deletion size was approximately 5 kbp. A DNA fragment located approximately 18 kbp from the deletion site was inserted into the deletion site.

Table 2
Summary of *gpt* mutations derived from the GDL1 cells

Type of mutation	Control		MMC		*P* value[a]
	No. of mutants (%)	Specific MF[b] ($\times 10^{-6}$)	No. of mutants (%)	Specific MF[b] ($\times 10^{-6}$)	
Base substitution/single					
Transition					
G:C → A:T	13 (28.3)	6.4	7 (15.6)	12.3	0.18
A:T → G:C	3 (6.5)	1.5	2 (4.4)	3.5	0.31
Transversion					
G:C → T:A	8 (17.4)	3.9	15 (33.3)	26.3	<0.0001
G:C → C:G	1 (2.2)	0.5	1 (2.2)	1.8	0.40
A:T → T:A	4 (8.7)	2.0	0 (0.0)	0.0	0.58
A:T → C:G	5 (10.9)	2.5	1 (2.2)	1.8	1.00
Insertion					
+1A	2 (4.3)	1.0	0 (0.0)	0.0	1.00
+1T	3 (6.5)	1.5	2 (4.4)	3.5	0.31
>+2 bp	0 (0.0)	0.0	2 (4.4)	3.5	<0.05
Deletion					
−1A	1 (2.2)	0.5	0 (0.0)	0.0	1.00
−1G	2 (4.3)	1.0	0 (0.0)	0.0	1.00
−1C	2 (4.3)	1.0	2 (4.4)	3.5	0.22
>−2 bp	1 (2.2)	0.5	4 (8.9)	7.0	<0.05
Base substitution/tandem					
GG:CC → TC:AG	0 (0.0)	0.0	2 (4.4)	3.5	<0.05
GG:CC → TT:AA	0 (0.0)	0.0	2 (4.4)	3.5	<0.05
CG:GC → AA:TT	0 (0.0)	0.0	1 (2.2)	1.8	0.22
Others	1 (2.2)	0.5	4 (8.9)	7.0	<0.05
Total	46 (100)	22.7	45 (100)	78.9	<0.0001

[a] *P* values were determined using Fisher's exact test according to Carr and Gorelick [22].
[b] Specific MF was calculated by multiplying the total mutation frequency by the ratio of each type of mutation to the total mutation.

complex mutation, i.e., gM1-6 (Fig. 7). In this complex mutant, three DNA fragments were inserted into position 158–168 of the *gpt* gene, and the direction and the order of the inserted fragments were different from those of the original sequences. The original locations of fragment 1 (335 bp), fragment 2 (1092 bp), and fragment 3 (133 bp) were 17, 13, and 22 kbp, respectively, from the inserted position. A mutation in the control group of this class was a sequence substitution of 5′-CCG-3′ to 5′-ACC-3′ in position 278–280.

4. Discussion

Significant and dose-related increases in Spi$^-$ and *gpt* MFs of the GDL1 cells were observed after treatment with MMC (Fig. 2, Tables 1 and 2). In the in vivo experiment using *gpt* delta mice exposed to MMC [8], statistically significant increases of large deletion mutations (class I, Table 3) in Spi$^-$ mutants and tandem base substitutions at the 5′-GG-3′ or 5′-CG-3′ sequence (Table 4) in *gpt* mutants were seen. These mutations were also predominantly induced in GDL1 cells by MMC (Tables 3 and 4). In addition, MMC-induced complex mutations (class IV) in Spi$^-$ mutants and single base substitutions at G:C bp in the *gpt* mutants were observed in the GDL1 cells (Tables 3 and 4). Increase of these mutations was not observed in *gpt* delta mice treated with MMC [8]. Single base substitutions at G:C bp induced by MMC were also reported in another mammalian cell in vitro [25]. Monoadducts of MMC are probably responsible for single base mutations [26], and adducts are preferentially formed in the 5′-CG-3′ and 5′-GG-3′ sequences [23,24]. In fact, most of the single base substitutions were observed at guanines at the 5′-CG-3′ or 5′-GG-3′ sequences (Fig. 6). The GDL1 cell line was established from the genetic modification of introducing an artificially constructed expression unit for the SV40 T antigen gene into lung fibroblasts of *gpt* delta mice. The SV40 T antigen can immortalize fibroblasts through formation of complexes with p53 and interruption of p53-dependent growth suppression [27–29]. Hence, the normal function of p53 might be lost in the GDL1 cells.

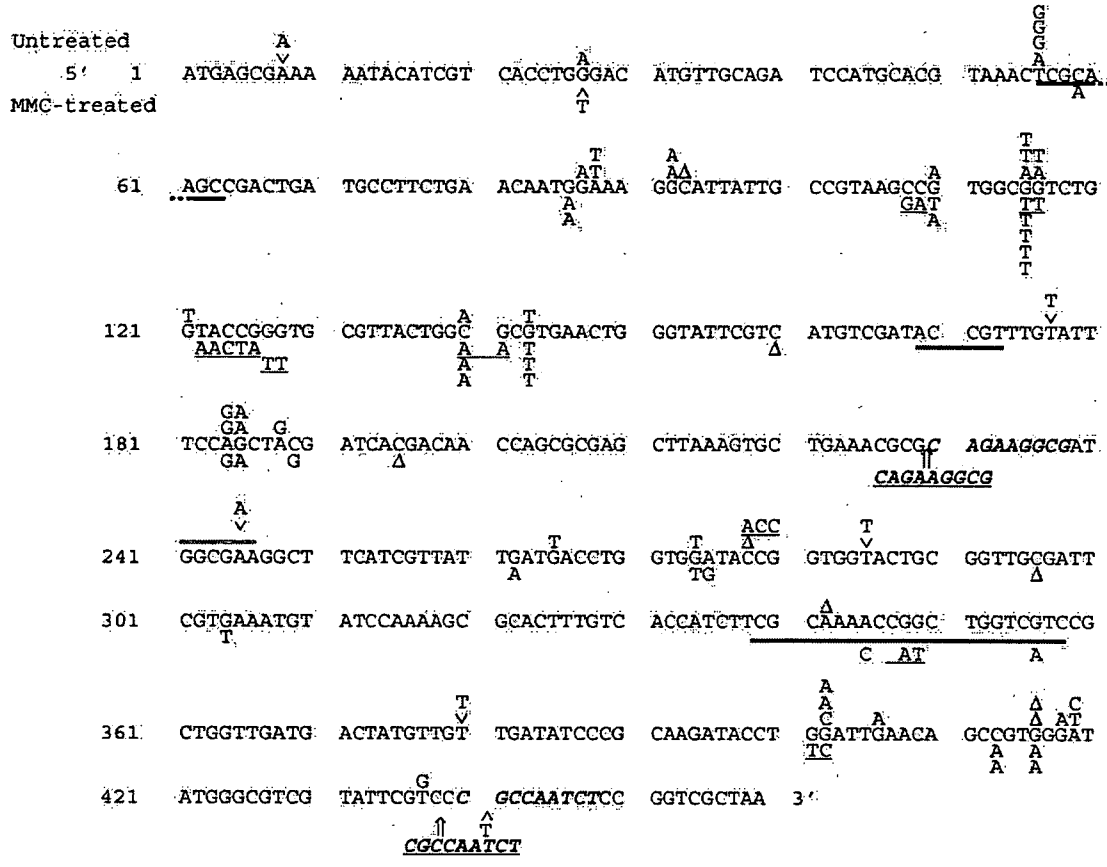

Fig. 6. Mutations in the *gpt* gene obtained from MMC-treated and untreated GDL1 cells. The sequence from top to the bottom represents the coding region of the *gpt* gene. Mutations shown above the sequence are from untreated cells and below from cells treated with MMC. (Δ and ∧) Single base deletions and one base insertion, respectively. Tandem base substitutions and sequence substitutions are underlined. Bars represent deleted sequences in deletion mutations. Inserted sequences are underlined and insertion positions are shown with arrows. The repeated sequences are shown in italicized boldface. In MMC-treated cells, a 329-bp deletion in nucleotide −3 to 326 (−3 indicates 3 bp prior to the first base of the first codon) and a 565-bp deletion accompanied by 1 bp insertion in position 11–575, and a complex rearrangement are not represented in Fig. 6 (see Fig. 7 for a complex rearrangement). One *gpt* mutant in untreated cells had two G:C to T:A mutations in nucleotide 121 and 143.

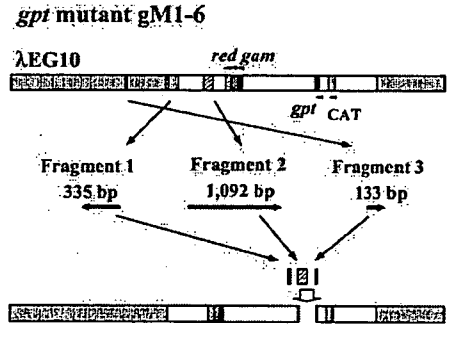

Fig. 7. Rearrangement induced in the *gpt* mutant derived from MMC-treated GDL1 cells. In *gpt* mutant gM1-6, three DNA fragments, fragment 1 (335 bp), fragment 2 (1092 bp), and fragment 3 (133 bp), were inserted into position of 158–168 of the *gpt* gene, and the directions and orders of the inserted fragments were different from that of the original sequence.

The p53 gene plays an important role in nucleotide excision repair (NER) [30–33] and NER activity decreased in cell lines transformed with the SV40 T antigen [34] and papillomavirus E6 genes [35]. Therefore, the potency of p53-dependent DNA repair pathways including NER might be different between GDL1 cells and *gpt* delta mice, which could account for the induction of single base substitutions and complex mutations (see below) in GDL1 cells.

Five complex mutations of Spi$^-$ (Fig. 5) and one rearranged mutant of *gpt* (Fig. 7) were observed in MMC-treated GDL1 cells. Comparison of the Spi$^-$ mutant in *p53*$^{+/+}$ and *p53*$^{-/-}$ *gpt* delta mice exposed to carbon-ion irradiation indicated that the induction of complex rearrangements was significantly accelerated by p53-knockout in the kidney, where p53 is highly expressed, but not in the liver, where p53 is weakly

Table 3
Comparison of specific MF of Spi⁻ mutations between *gpt* delta mice and GDL1 cells

Type of mutation	Class of mutation	Control			MMC			
		gpt delta mice[a]	GDL1 cells		*gpt* delta mice[a]		GDL1 cells	
		Specific MF[b] ($\times 10^{-6}$)	Specific MF[b] ($\times 10^{-6}$)	*P* value[c,d]	Specific MF[b] ($\times 10^{-6}$)	*P* value[c,e]	Specific MF[b] ($\times 10^{-6}$)	*P* value[c,f]
Large deletion (>1 kbp)								
With microhomology	I-A	0.0	4.2	<0.0001	1.6	<0.001	17.6	<0.01
Without microhomology	I-B	0.1	0.0	1.00	0.6	0.19	5.9	<0.05
Midsize deletion (2 bp to 1 kbp)	II	0.0	1.2	<0.05	0.2	0.47	7.8	<0.05
Single base deletion								
At run sequence	III-A	1.4	17.3	<0.0001	1.4	1.00	33.2	0.06
At non-run sequence	III-B	0.1	1.2	0.08	0.2	1.00	0.0	1.00
Complex mutation	IV	0.0	0.0	–	0.0	–	9.8	<0.001
Miscellaneous mutation	V	0.1	1.8	<0.05	1.3	<0.05	11.7	<0.01
Unidentified		0.0	0.0	–	0.0	–	2.0	0.24
Total		1.8	25.6	<0.0001	5.2	<0.01	88.0	<0.0001

[a] Data previously reported by us [8].
[b] Specific MF was calculated by multiplying the total mutation frequency by the ratio of each type of mutation to the total mutation.
[c] *P* values were determined using Fisher's exact test according to Carr and Gorelick [22].
[d] Comparison between the control group of *gpt* delta mice and control group of GDL1 cells.
[e] Comparison between the control group of *gpt* delta mice and MMC-treated group of *gpt* delta mice.
[f] Comparison between the control group of GDL1 cells and MMC-treated group of GDL1 cells.

expressed [36]. Thus, a p53 defect by the recombinant SV40 T antigen may cause the DNA rearrangement occurring in GDL1 cells. The breakage-fusion bridge cycle reported in p53 deficient mammalian cells might involve in the DNA rearrangement observed in GDL1 cells [37,38].

It is interesting and surprising to note that Spi⁻ mutant sM1-9 has a DNA fragment from chromosome

Table 4
Comparison of specific MF of *gpt* mutations between *gpt* delta mice and GDL1 cells

Type of mutation	Control			MMC			
	gpt delta mice[a]	GDL1 cells		*gpt* delta mice[a]		GDL1 cells	
	Specific MF[b] ($\times 10^{-6}$)	Specific MF[b] ($\times 10^{-6}$)	*P* value[c,d]	Specific MF[b] ($\times 10^{-6}$)	*P* value[c,e]	Specific MF[b] ($\times 10^{-6}$)	*P* value[c,f]
Base substitution/single							
At G:C	5.4	10.9	<0.05	6.6	0.47	40.3	<0.0001
At A:T	1.7	5.9	<0.01	1.9	0.75	5.3	1.00
Insertion	0.0	2.5	<0.01	0.0	–	7.0	0.12
Deletion	1.1	3.0	0.10	0.9	0.30	10.5	<0.05
Base substitution/tandem	0.0	0.0	–	3.3	<0.001	8.8	<0.001
Others	0.0	0.5	0.35	1.4	<0.05	7.0	<0.05
Total	8.2	22.7	<0.0001	14.1	<0.0001	78.9	<0.0001

[a] Data previously reported by us [8].
[b] Specific MF was calculated by multiplying the total mutation frequency by the ratio of each type of mutation to the total mutation.
[c] *P* values were determined using Fisher's exact test according to Carr and Gorelick [22].
[d] Comparison between the control group of *gpt* delta mice and control group of GDL1 cells.
[e] Comparison between the control group of *gpt* delta mice and MMC-treated group of *gpt* delta mice.
[f] Comparison between the control group of GDL1 cells and MMC-treated group of GDL1 cells.